

Yukawa textures and charged Higgs boson phenomenology in the type-III two-Higgs-doublet model

J. L. Díaz-Cruz,^{1,*} J. Hernández-Sánchez,^{2,†} S.

Moretti,^{3,‡} R. Noriega-Papaqui,^{4,§} and A. Rosado^{5,¶}

¹*Fac. de Cs. Físico-Matemáticas, BUAP. Apdo. Postal 1364, C.P. 72000 Puebla, Pue., México, and Dual C-P Institute of High Energy Physics, México.*

²*Fac. de Cs. de la Electrónica, BUAP, Av. San Claudio y 18 Sur, C.P. 72500 Puebla, Pue., México, and Dual C-P Institute of High Energy Physics, México.*

³*School of Physics and Astronomy, University of Southampton, Highfield, Southampton SO17 1BJ, UK.*

⁴*Centro de Investigación en Matemáticas, Universidad Autónoma del Estado de Hidalgo, Carr. Pachuca-Tulancingo Km. 4.5, C.P. 42184, Pachuca, Hgo., México, and Dual C-P Institute of High Energy Physics, México.*

⁵*Instituto de Física, BUAP. Apdo. Postal J-48, C.P. 72570 Puebla, Pue., México.*

(Dated: October 28, 2018)

We discuss the implications of assuming a four-zero Yukawa texture for the properties of the charged Higgs boson within the context of the general 2-Higgs Doublet Model of Type III. We begin by presenting a detailed analysis of the charged Higgs boson couplings with heavy quarks and the resulting pattern for its decays. The production of charged Higgs bosons is also sensitive to the modifications of its couplings, so that we also evaluate the resulting effects on the top decay $t \rightarrow bH^+$ as well as on ‘direct’ $c\bar{b} \rightarrow H^+ + c$. c. and ‘indirect’ $q\bar{q}, gg \rightarrow t\bar{b}H^+ + c$. c. production. Significant scope exists at the Large Hadron Collider for several H^\pm production and decay channels combined to enable one to distinguish between such a model and alternative 2-Higgs doublet scenarios.

PACS numbers: 12.60.Cn, 12.60.Fr, 11.30.Er

*Electronic address: jldiaz@cfm.buap.mx

†Electronic address: jaimeh@ece.buap.mx

‡Electronic address: stefano@soton.ac.uk

§Electronic address: rnoriega@uaeh.edu.mx

¶Electronic address: rosado@sirio.ifuap.buap.mx

I. INTRODUCTION

Detecting a charged Higgs boson during the imminent Large Hadron Collider (LHC) experimental running would constitute a clear evidence of physics beyond the Standard Model (SM) [1]. Charged Higgs bosons appear in many well motivated extensions of the SM, whose phenomenology has been widely studied over the years [2, 3, 4]. In particular, 2-Higgs Doublet Models (2HDMs), in both Supersymmetry (SUSY) and non-SUSY versions [5, 6], can be considered as a prototype of a Higgs sector that includes a charged Higgs boson (H^\pm). It is expected that the LHC will allow us to test the mechanism of Electro-Weak Symmetry Breaking (EWSB) and, in particular, to probe the properties of charged Higgs bosons, which represent a unique probe of a weakly-interacting theory, as is the case of the Minimal Supersymmetric Standard Model (MSSM) [5] and general 2HDMs of Type I, II, III and IV (2HDM-I, 2HDM-II, 2HDM-III and 2HDM-IV) [7], or whether strongly-interacting scenarios are instead realized, like in the old Technicolor models or similar ones discussed more recently [8]. Ultimately, while many analyses in this direction can be carried out at the LHC, it will be a future International Linear Collider (ILC) [9] or Compact Linear Collider (CLIC) [10] which will have the definite word about exactly which mechanism of mass generation and which realization of it occurs in Nature.

The 2HDM-II has been quite attractive to date, in part because it coincides with the Higgs sector of the MSSM, wherein each Higgs doublet couples to the u - or d -type fermions separately¹. However, this is only valid at tree-level [12]. When radiative effects are included, it turns out that the MSSM Higgs sector corresponds to the most general version of the 2HDM, namely the 2HDM-III, whereby both Higgs fields couple to both quarks and leptons. Thus, we can consider the 2HDM-III as a generic description of physics at a higher scale (of order TeV or maybe even higher), whose low energy imprints are reflected in the Yukawa coupling structure. With this idea in mind, some of us have presented a detailed study of the 2HDM-III Yukawa Lagrangian [13], under the assumption of a specific texture pattern [14], which generalizes the original model of Ref. [15]. Phenomenological implications of this model for the neutral Higgs sector, including Lepton Flavour Violation (LFV) and/or Flavour Changing Neutral Currents (FCNCs) have been presented in a previous work [16]. Here, we are interested in extending such an approach to investigate charged Higgs boson phenomenology: namely, we want to study the implications of this Yukawa texture for the charged Higgs boson properties (masses and couplings) and discuss in detail the resulting

¹ Notice that there exist significant differences between the 2HDM-II and MSSM though, when it comes to their mass/coupling configurations and possible Higgs signals [11].

pattern of charged Higgs boson decays and main production reactions at the LHC.

Decays of charged Higgs bosons have been studied in the literature, including the radiative modes $W^\pm\gamma, W^\pm Z^0$ [17], mostly within the context of the 2HDM-II or its SUSY incarnation (i.e., the MSSM), but also by using an effective Lagrangian extension of the 2HDM [18] and, more recently, within an extension of the MSSM with one Complex Higgs Triplet (MSSM+1CHT) [19, 20]. Charged Higgs boson production at hadron colliders was studied long ago [21] and, more recently, systematic calculations of production processes at the LHC have been presented [22].

Current bounds on the mass of a charged Higgs boson have been obtained at Tevatron, by studying the top decay $t \rightarrow b H^+$, which already eliminates large regions of the parameter space [23], whereas LEP2 bounds imply that, approximately, $m_{H^+} > 80$ GeV [24, 25], rather model independently. Concerning theoretical limits, tree-level unitarity bounds on the 2HDM Higgs masses have been studied in generic 2HDMs and in particular an upper limit for the charged Higgs mass of 800 GeV or so can be obtained, according to the results of Ref. [26].

This paper is organized as follows. In section II, we discuss the Higgs-Yukawa sector of the 2HDM-III, in particular, we derive the expressions for the charged Higgs boson couplings to heavy fermions. Then, in section III, we derive the expressions for the decays $H^+ \rightarrow f_i \bar{f}_j$ and numerical results are presented for some 2HDM-III scenarios, defined for phenomenological purposes. A discussion of the main production mechanisms at the LHC is presented in section IV. These include the top decay $t \rightarrow b H^+$ as well as s -channel production of charged Higgs bosons through $c\bar{b}(\bar{c}b)$ -fusion [27] and the multi-body more $q\bar{q}, gg \rightarrow t\bar{b}H^- + \text{c.c.}$ (charge conjugated). These mechanisms depend crucially on the parameters of the underlying model and large deviations should be expected in the 2HDM-III with respect to the 2HDM-II. Actual LHC event rates are given in section V. Finally, we summarize our results and present the conclusions in section VI. Notice that in carrying out this plan, unlike other references [28, 29], where the 2HDM-II and the 2HDM-III appear as different structures, we shall consider here that, under certain limits, the 2HDM-III reduces to the 2HDM-II and, therefore, that the properties of the charged Higgs bosons change continuously from one model to the other.

II. THE CHARGED HIGGS BOSON LAGRANGIAN AND THE FERMIONIC COUPLINGS

We shall follow Refs. [13, 16], where a specific four-zero texture has been implemented for the Yukawa matrices within the 2HDM-III. This allows one to express the couplings of the neutral and

charged Higgs bosons in terms of the fermion masses, Cabibbo-Kobayashi-Maskawa (CKM) mixing angles and certain dimensionless parameters, which are to be bounded by current experimental constraints. Thus, in order to derive the interactions of the charged Higgs boson, the Yukawa Lagrangian is written as follows:

$$\mathcal{L}_Y = Y_1^u \bar{Q}_L \tilde{\Phi}_1 u_R + Y_2^u \bar{Q}_L \tilde{\Phi}_2 u_R + Y_1^d \bar{Q}_L \Phi_1 d_R + Y_2^d \bar{Q}_L \Phi_2 d_R, \quad (1)$$

where $\Phi_{1,2} = (\phi_{1,2}^+, \phi_{1,2}^0)^T$ refer to the two Higgs doublets, $\tilde{\Phi}_{1,2} = i\sigma_2 \Phi_{1,2}^*$, Q_L denotes the left-handed fermion doublet, u_R and d_R are the right-handed fermions singlets and, finally, $Y_{1,2}^{u,d}$ denote the (3×3) Yukawa matrices. Similarly, one can write the corresponding Lagrangian for leptons.

After spontaneous EWSB and including the diagonalizing matrices for quarks and Higgs bosons², the interactions of the charge Higgs boson H^+ with quark pairs acquire the following form:

$$\begin{aligned} \mathcal{L}^{\bar{q}_i q_j H^+} = & \frac{g}{2\sqrt{2}M_W} \sum_{l=1}^3 \bar{u}_i \left\{ (V_{\text{CKM}})_{il} \left[\tan \beta m_{d_l} \delta_{lj} - \sec \beta \left(\frac{\sqrt{2}M_W}{g} \right) (\tilde{Y}_2^d)_{lj} \right] \right. \\ & + \left[\cot \beta m_{u_i} \delta_{il} - \csc \beta \left(\frac{\sqrt{2}M_W}{g} \right) (\tilde{Y}_1^u)_{il}^\dagger \right] (V_{\text{CKM}})_{lj} \\ & + (V_{\text{CKM}})_{il} \left[\tan \beta m_{d_l} \delta_{lj} - \sec \beta \left(\frac{\sqrt{2}M_W}{g} \right) (\tilde{Y}_2^d)_{lj} \right] \gamma^5 \\ & \left. - \left[\cot \beta m_{u_i} \delta_{il} - \csc \beta \left(\frac{\sqrt{2}M_W}{g} \right) (\tilde{Y}_1^u)_{il}^\dagger \right] (V_{\text{CKM}})_{lj} \gamma^5 \right\} d_j H^+, \end{aligned} \quad (2)$$

where V_{CKM} denotes the mixing matrices of the quark sector (and similarly for the leptons). The term proportional to δ_{ij} corresponds to the contribution that would arise within the 2HDM-II, while the terms proportional to \tilde{Y}_2^d and \tilde{Y}_1^u denote the new contributions from the 2HDM-III. These contributions, depend on the rotated matrices: $\tilde{Y}_n^q = O_q^T P_q Y_n^q P_q^\dagger O_q$ ($n = 1$ when $q = u$, and $n = 2$ when $q = d$), where O_q is the diagonalizing matrix, while P_q includes the phases of the Yukawa matrix. In order to evaluate \tilde{Y}_n^q we shall consider that all Yukawa matrices have the Hermitian four-zero texture form [14], and the quark masses have the same form, which are given by:

$$M^q = \begin{pmatrix} 0 & C_q & 0 \\ C_q^* & \tilde{B}_q & B_q \\ 0 & B_q^* & A_q \end{pmatrix} \quad (q = u, d). \quad (3)$$

² The details of both diagonalizations are presented in Ref. [13]

This is called a four-zero texture because one assumes that the Yukawa matrices are Hermitian, therefore each u and d type Yukawa matrix contains two independent zeros. According to current analyzes this type of texture satisfies the experimental constraints and at the same time it permits to derive analytical expressions for the Higgs boson fermion couplings.

To diagonalize M^q , we use the matrices O_q and P_q , in the following way [14]:

$$\bar{M}^q = O_q^T P_q M^q P_q^\dagger O_q. \quad (4)$$

Then, one can derive a better approximation for the product $O_q^T P_q Y_n^q P_q^\dagger O_q$, expressing the rotated matrix \tilde{Y}_n^q , in the form

$$[\tilde{Y}_n^q]_{ij} = \frac{\sqrt{m_i^q m_j^q}}{v} [\tilde{\chi}_n^q]_{ij} = \frac{\sqrt{m_i^q m_j^q}}{v} [\chi_n^q]_{ij} e^{i\theta_{ij}^q}. \quad (5)$$

In order to perform our phenomenological study, we find it convenient to rewrite the Lagrangian given in Eq. (2) in terms of the coefficients $[\tilde{\chi}_n^q]_{ij}$, as follows:

$$\begin{aligned} \mathcal{L}^q = & \frac{g}{2\sqrt{2}M_W} \sum_{l=1}^3 \bar{u}_i \left\{ (V_{\text{CKM}})_{il} \left[\tan \beta m_{d_l} \delta_{lj} - \frac{\sec \beta}{\sqrt{2}} \sqrt{m_{d_l} m_{d_j}} \tilde{\chi}_{lj}^d \right] \right. \\ & + \left[\cot \beta m_{u_i} \delta_{il} - \frac{\csc \beta}{\sqrt{2}} \sqrt{m_{u_i} m_{u_l}} \tilde{\chi}_{il}^u \right] (V_{\text{CKM}})_{lj} \\ & + (V_{\text{CKM}})_{il} \left[\tan \beta m_{d_l} \delta_{lj} - \frac{\sec \beta}{\sqrt{2}} \sqrt{m_{d_l} m_{d_j}} \tilde{\chi}_{lj}^d \right] \gamma^5 \\ & \left. - \left[\cot \beta m_{u_i} \delta_{il} - \frac{\csc \beta}{\sqrt{2}} \sqrt{m_{u_i} m_{u_l}} \tilde{\chi}_{il}^u \right] (V_{\text{CKM}})_{lj} \gamma^5 \right\} d_j H^+, \end{aligned} \quad (6)$$

where we have redefined $[\tilde{\chi}_1^u]_{ij} = \tilde{\chi}_{ij}^u$ and $[\tilde{\chi}_2^d]_{ij} = \tilde{\chi}_{ij}^d$. Then, from Eq. (6), the couplings $\bar{u}_i d_j H^+$ and $u_i \bar{d}_j H^-$ are given by:

$$g_{H^+ \bar{u}_i d_j} = -\frac{ig}{2\sqrt{2}M_W} (S_{ij} + P_{ij} \gamma_5), \quad g_{H^- u_i \bar{d}_j} = -\frac{ig}{2\sqrt{2}M_W} (S_{ij} - P_{ij} \gamma_5), \quad (7)$$

where S_{ij} and P_{ij} are defined as:

$$\begin{aligned} S_{ij} = & \sum_{l=1}^3 (V_{\text{CKM}})_{il} \left[\tan \beta m_{d_l} \delta_{lj} - \frac{\sec \beta}{\sqrt{2}} \sqrt{m_{d_l} m_{d_j}} \tilde{\chi}_{lj}^d \right] \\ & + \left[\cot \beta m_{u_i} \delta_{il} - \frac{\csc \beta}{\sqrt{2}} \sqrt{m_{u_i} m_{u_l}} \tilde{\chi}_{il}^u \right] (V_{\text{CKM}})_{lj}, \\ P_{ij} = & \sum_{l=1}^3 (V_{\text{CKM}})_{il} \left[\tan \beta m_{d_l} \delta_{lj} - \frac{\sec \beta}{\sqrt{2}} \sqrt{m_{d_l} m_{d_j}} \tilde{\chi}_{lj}^d \right] \\ & - \left[\cot \beta m_{u_i} \delta_{il} - \frac{\csc \beta}{\sqrt{2}} \sqrt{m_{u_i} m_{u_l}} \tilde{\chi}_{il}^u \right] (V_{\text{CKM}})_{lj}. \end{aligned} \quad (8)$$

As it was discussed in Ref. [13], most low-energy processes imply weak bounds on the coefficients $\tilde{\chi}_{ij}^q$, which turn out to be of $O(1)$. However, some important constraints on $\tan \beta$ have started to appear, based on B -physics [30]. In order to discuss these results we find convenient to generalize the notation of Ref. [31] and define the couplings $\bar{u}_i d_j H^+$ and $u_i \bar{d}_j H^-$ in terms of the matrices X_{ij} , Y_{ij} and Z_{ij} (for leptons). In our case these matrices are given by:

$$\begin{aligned} X_{lj} &= \left[\tan \beta \delta_{lj} - \frac{\sec \beta}{\sqrt{2}} \sqrt{\frac{m_{d_j}}{m_{d_l}}} \tilde{\chi}_{lj}^d \right], \\ Y_{il} &= \left[\cot \beta \delta_{il} - \frac{\csc \beta}{\sqrt{2}} \sqrt{\frac{m_{u_l}}{m_{u_i}}} \tilde{\chi}_{il}^u \right]. \end{aligned} \quad (9)$$

where X_{lj} and Y_{il} are related with S_{ij} and P_{ij} defined in the Eq. (8) as follows:

$$\begin{aligned} S_{ij} &= \sum_{l=1}^3 [(V_{\text{CKM}})_{il} m_{d_l} X_{lj} + m_{u_i} Y_{il} (V_{\text{CKM}})_{lj}], \\ P_{ij} &= \sum_{l=1}^3 [(V_{\text{CKM}})_{il} m_{d_l} X_{lj} - m_{u_i} Y_{il} (V_{\text{CKM}})_{lj}]. \end{aligned} \quad (10)$$

The 33 elements of these matrices reduce to the expressions for the parameters X, Y, Z ($= X_{33}, Y_{33}, Z_{33}$) used in Ref.[31]. Based on the analysis of $B \rightarrow X_s \gamma$ [31, 32], it is claimed that $X \leq 20$ and $Y \leq 1.7$ for $m_{H^+} > 250$ GeV, while for a lighter charged Higgs boson mass, $m_{H^+} \sim 200$ GeV, one gets $(X, Y) \leq (18, 0.5)$. Fig. 1 shows the values of (X, Y) as a function of $\tan \beta$ within our model. Thus, we find important bounds: $|\chi_{33}^{u,d}| \lesssim 1$ for $0.1 < \tan \beta \leq 70$. Although in our model there are additional contributions (for instance from c -quarks, which are proportional to X_{23}), they are not relevant because the Wilson coefficients in the analysis of $B \rightarrow X_s \gamma$ are functions of m_c^2/M_W^2 or $m_c^2/m_{H^+}^2$ [33], that is, negligible when compared to the leading X_{33} effects, whose Wilson coefficients depend on m_t^2/M_W^2 or $m_t^2/m_{H^+}^2$. Other constraints on the charged Higgs mass and $\tan \beta$, based on Δa_μ , the ρ parameter, as well as B -decays into the tau lepton, can be obtained [34, 35]. For instance, as can be read from Ref.[36], one has that the decay $B \rightarrow \tau \nu$, implies a constraint such that for $m_{H^+} = 200$ (300) GeV, values of $\tan \beta$ less than about 30 (50) are still allowed, within MSSM or 2HDM-III: However, these constraints can only be taken as estimates, as it is likely that they would be modified for 2HDM-III. In summary, we find that low energy constraints still allow to have $\tilde{\chi}_{ij}^q = O(1)$ ³.

³ A more detailed analysis that includes the most recent data is underway [37].

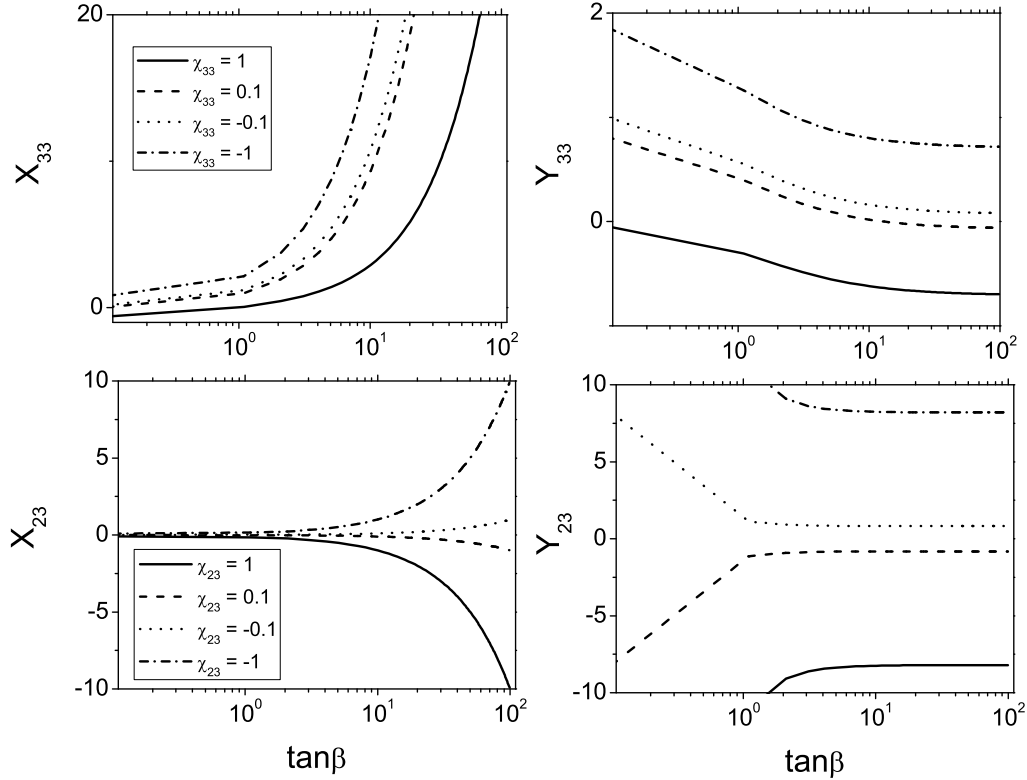


FIG. 1: The figure shows X_{33} , Y_{33} , X_{23} and Y_{23} vs. $\tan\beta$, taking $\tilde{\chi}_{3,3}^{u,d} = 1$ (solid), $\tilde{\chi}_{3,3}^{u,d} = 0.1$ (dashes), $\tilde{\chi}_{3,3}^{u,d} = -0.1$ (dots), $\tilde{\chi}_{3,3}^{u,d} = -1$ (dashes-dots).

III. DECAYS OF THE CHARGED HIGGS BOSON

Let us now discuss the decay modes of the charged Higgs boson within our model. Hereafter, we shall refer to four benchmark scenarios, namely. (i) **Scenario A**: $\tilde{\chi}_{ij}^u = 1$, $\tilde{\chi}_{ij}^d = 1$; (ii) **Scenario B**: $\tilde{\chi}_{ij}^u = 0.1$, $\tilde{\chi}_{ij}^d = 1$; (iii) **Scenario C**: $\tilde{\chi}_{ij}^u = 1$, $\tilde{\chi}_{ij}^d = 0.1$; (iv) **Scenario D**: $\tilde{\chi}_{ij}^u = 0.1$, $\tilde{\chi}_{ij}^d = 0.1$. We have performed the numerical analysis of charged Higgs boson decays by taking $\tan\beta = 0.1, 1, 15, 70$ and varying the charged Higgs boson mass within the interval $100 \text{ GeV} \leq m_{H^\pm} \leq 1000 \text{ GeV}$, further fixing $m_{h^0} = 120 \text{ GeV}$, $m_{A^0} = 300 \text{ GeV}$ and the mixing angle at $\alpha = \pi/2$.

The condition $\frac{\Gamma_{H^+}}{m_{H^+}} < \frac{1}{2}$ in the frame of the 2HDM-II implies $\frac{\Gamma_{H^+}}{m_{H^+}} \approx \frac{3G_F m_t^2}{4\sqrt{2}\pi \tan\beta^2}$ which leads to $0.3 \lesssim \tan\beta \lesssim 130$. However, in the 2HDM-III we have that $\frac{\Gamma_{H^+}}{m_{H^+}} \approx \frac{3G_F m_t^2}{4\sqrt{2}\pi \tan\beta^2} \left(\frac{1}{1 - \frac{\tilde{\chi}_{33}^u}{\sqrt{2}\cos\beta}} \right)^2$, we have checked numerically that this leads to $0.08 < \tan\beta < 200$ when $|\tilde{\chi}_{33}^u| \approx 1$ and $0.3 < \tan\beta <$

130 as long as $|\tilde{\chi}_{33}^u| \rightarrow 0$ recovering the result for the case of the 2HDM-II [7, 38]. In this sense, if we consider the constraints imposed by the perturbativity bound, a portion of the low $\tan\beta$ appearing in some graphs would be excluded. However, we have decided to keep that range both to show the behaviour of the quantities of interest, and also because we have to keep in mind that such criteria (perturbativity) should be taken as an order of magnitude constraint.

The expressions for the charged Higgs boson decay widths $H^+ \rightarrow u_i \bar{d}_j$ are of the form:

$$\Gamma(H^+ \rightarrow u_i \bar{d}_j) = \frac{3g^2}{32\pi M_W^2 m_{H^+}^3} \lambda^{1/2}(m_{H^+}^2, m_{u_i}^2, m_{d_j}^2) \times \left(\frac{1}{2} \left[m_{H^+}^2 - m_{u_i}^2 - m_{d_j}^2 \right] (S_{ij}^2 + P_{ij}^2) - m_{u_i} m_{d_j} (S_{ij}^2 - P_{ij}^2) \right), \quad (11)$$

where λ is the usual kinematic factor $\lambda(a, b, c) = (a - b - c)^2 - 4bc$. When we replace $\tilde{\chi}_{ud} \rightarrow 0$, the formulae of the decays width become those of the 2HDM-II: see, e.g., Ref. [2]. Furthermore, the expressions for the charged Higgs boson decay widths of the bosonic modes remain the same as in the 2HDM-II. Then the results for the Branching Ratios (BRs) are shown in Figs. 2–8, and have the following characteristics.

Scenario A. In Fig. 2(a) we present the BRs for the channels $H^+ \rightarrow t\bar{b}$, $c\bar{b}$, $t\bar{s}$, $\tau^+\nu_\tau$, W^+h^0 , W^+A^0 as a function of m_{H^+} , for $\tan\beta = 0.1$ and fixing $m_{h^0} = 120$ GeV, $m_{A^0} = 300$ GeV and the mixing angle $\alpha = \pi/2$. When $m_{H^+} < 175$ GeV, we can see that the dominant decay of the charged Higgs boson is via the mode $c\bar{b}$, with $\text{BR}(H_i^+ \rightarrow c\bar{b}) \approx 1$, which will have important consequences for charged Higgs boson production through $c\bar{b}$ -fusion at the LHC and may serve as a distinctive feature of this model. For the case $175 \text{ GeV} < m_{H^+} < 180$ GeV the mode $t\bar{s}$ is relevant, which it is also very different from the 2HDM-II and becomes an interesting phenomenological consequence of the 2HDM-III. We can also observe that, for $m_{H^+} > 180$ GeV, the decay mode $t\bar{b}$ is dominant (as in the 2HDM-II). Now, from Fig. 2(b), where $\tan\beta = 1$, we find that the dominant decay mode is into $\tau^+\nu_\tau$ for the range $m_{H^+} < 175$ GeV, again for $175 \text{ GeV} < m_{H^+} < 180$ GeV the mode $t\bar{s}$ is the leading one, but for $180 \text{ GeV} < m_{H^+} < 600$ GeV, the decay channel W^+h^0 becomes relevant, whereas for the range $600 \text{ GeV} < m_{H^+}$ the mode W^+A^0 is dominant. It is convenient to mention that this sub-scenario is special for the mode $t\bar{b}$, because its decay width is zero at the tree-level, since the CKM contribution is canceled exactly with the terms of the four-zero texture implemented for the Yukawa coupling of the 2HDM-III. Then, see Fig. 2(c), for the case with $\tan\beta = 15$ one gets that $\text{BR}(H^+ \rightarrow \tau^+\nu_\tau) \approx 1$ when $m_{H^+} < 180$ GeV. However for $180 \text{ GeV} < m_{H^+} < 300$ GeV, the dominant decay of the charged Higgs boson is the mode $t\bar{b}$, while in the range $300 \text{ GeV} < m_{H^+}$, the decay channel W^+h^0 is also relevant. For $\tan\beta = 70$, we show in plot Fig. 2(d) that the dominant decay of the charged Higgs boson is the mode $\tau^+\nu_\tau$, when $m_{H^+} < 300$ GeV, but that, for 300

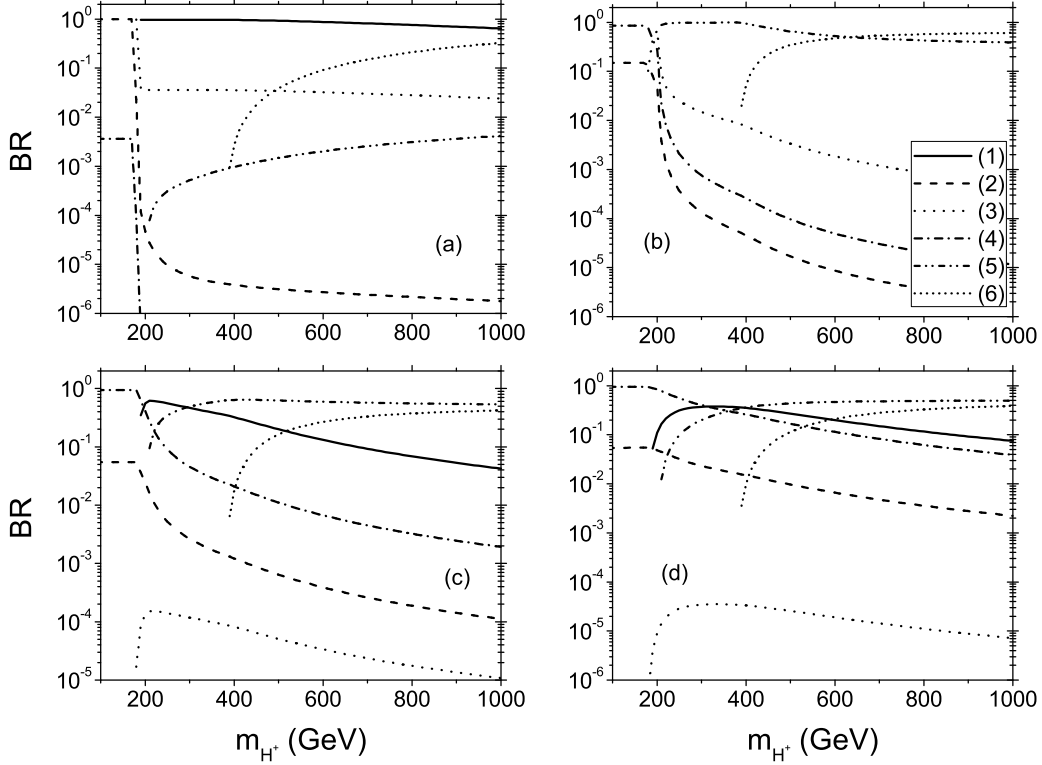


FIG. 2: The figure shows the BRs of the H^+ decaying into the principal modes in Scenario A, taking $\tilde{\chi}_{ij}^u = 1$, $\tilde{\chi}_{ij}^d = 1$, $m_{h^0} = 120$ GeV, $m_{A^0} = 300$ GeV and $\alpha = \pi/2$ for: (a) $\tan \beta = 0.1$, (b) $\tan \beta = 1$, (c) $\tan \beta = 15$, (d) $\tan \beta = 70$. The lines in each graph correspond to: (1) $\text{BR}(H^+ \rightarrow t\bar{b})$, (2) $\text{BR}(H^+ \rightarrow c\bar{b})$, (3) $\text{BR}(H^+ \rightarrow t\bar{s})$, (4) $\text{BR}(H^+ \rightarrow \tau^+\nu_\tau)$, (5) $\text{BR}(H^+ \rightarrow W^+h^0)$, (6) $\text{BR}(H^+ \rightarrow W^+A^0)$.

GeV $< m_{H^+} < 400$ GeV, the decay channel $t\bar{b}$ becomes the leading one, whereas for the range 400 GeV $< m_{H^+}$, the mode W^+h^0 is again dominant.

Scenario B. In Fig. 3, we present the BRs of the channels $H^+ \rightarrow t\bar{b}$, $c\bar{b}$, $t\bar{s}$, $\tau^+\nu_\tau$, W^+h^0 , W^+A^0 as a function of m_{H^+} . From Fig. 3(a), we observe that for $\tan \beta = 0.1$, when $m_{H^+} < 175$ GeV, the dominant decay of the charged Higgs boson is the mode $c\bar{b}$, with $\text{BR}(H_i^+ \rightarrow c\bar{b}) \approx 1$. When 175 GeV $< m_{H^+} < 180$ GeV the mode $t\bar{s}$ is important and for $m_{H^+} > 180$ GeV the decay mode $t\bar{b}$ becomes the leading one. From Fig. 3(b), we see that, for $\tan \beta = 1$, the dominant decay mode is now into $\tau^+\nu_\tau$ for $m_{H^+} < 175$ GeV, while in the range 175 GeV $< m_{H^+} < 180$ GeV the mode $t\bar{s}$ is relevant. For 180 GeV $< m_{H^+} < 500$ GeV the decay channel $t\bar{b}$ becomes the leading one, whereas for the range 500 GeV $< m_{H^+}$ the mode W^+A^0 is dominant. From Fig. 3(c), with $\tan \beta = 15$, one gets that $\text{BR}(H_i^+ \rightarrow \tau^+\nu_\tau) \approx 1$ for $m_{H^+} < 180$ GeV. For 180 GeV $< m_{H^+}$, the dominant decay of

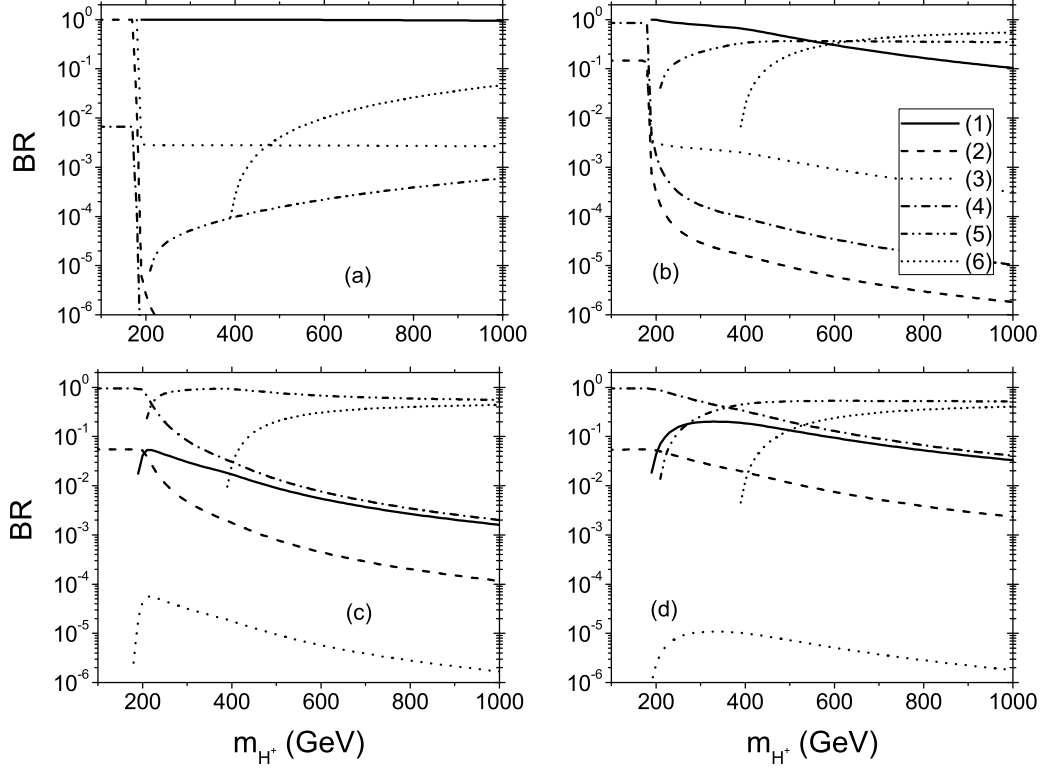


FIG. 3: The same as in Fig. 2 but taking $\tilde{\chi}_{ij}^u = 0.1$, $\tilde{\chi}_{ij}^d = 1$ (Scenario B).

the charged Higgs boson is instead the mode W^+h^0 . Then, for $\tan\beta = 70$, we show in Fig. 3(d) that the dominant decay of the charged Higgs state is via the mode $\tau^+\nu_\tau$ when $m_{H^+} < 350$ GeV while for $350 \text{ GeV} < m_{H^+}$ the decay channel W^+h^0 becomes the leading one.

Scenario C. In Fig. 4 we show the corresponding plots for the BRs of the channels $H^+ \rightarrow t\bar{b}$, $c\bar{b}$, $t\bar{s}$, $\tau^+\nu_\tau$, W^+h^0 , W^+A^0 as a function of m_{H^+} . For $\tan\beta = 0.1$, as one can see in Fig. 4(a), the mode $c\bar{b}$ is dominant when $m_{H^+} < 170$ GeV, but for $175 \text{ GeV} < m_{H^+} < 180$ GeV the mode $t\bar{s}$ is relevant, while for $180 \text{ GeV} < m_{H^+}$ the mode $t\bar{b}$ becomes dominant. For $\tan\beta = 1$, we observe from Fig. 4(b) that the dominant decay modes are: $\tau^+\nu_\tau$ in the range $m_{H^+} < 170$ GeV, $t\bar{s}$ for $175 \text{ GeV} < m_{H^+} < 180$ GeV, W^+h^0 for $180 \text{ GeV} < m_{H^+} < 600$ GeV and W^+A^0 when $600 \text{ GeV} < m_{H^+}$. For $\tan\beta = 15$, as shown in Fig. 4(c), the relevant decay channels are: $\tau^+\nu_\tau$ in the range $m_{H^+} < 180$ GeV, $t\bar{b}$ when $180 \text{ GeV} < m_{H^+} < 300$ GeV, W^+h^0 for $300 \text{ GeV} < m_{H^+}$. In Fig. 4(d), for $\tan\beta = 70$, we observe that $\tau^+\nu_\tau$ dominates when $m_{H^+} < 180$ GeV, but when $180 \text{ GeV} < m_{H^+} < 900$ GeV the mode $t\bar{b}$ is the leading one, whereas for $900 \text{ GeV} < m_{H^+}$ the mode

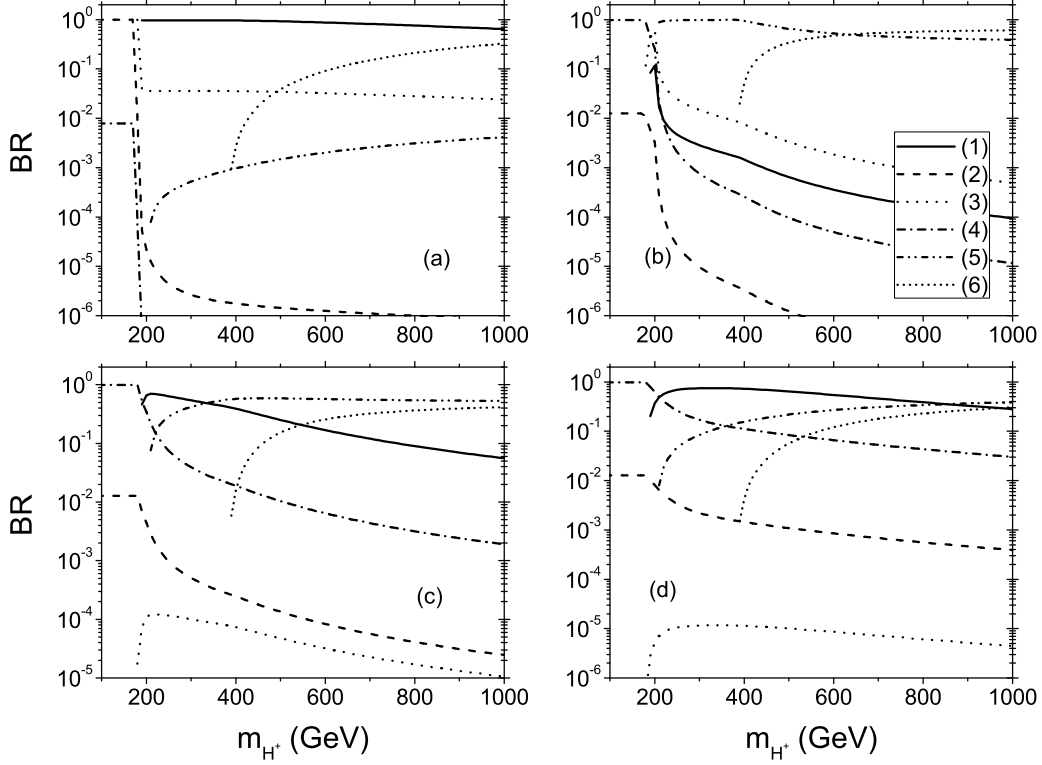


FIG. 4: The same as in Fig. 2, but taking $\tilde{\chi}_{ij}^u = 1$, $\tilde{\chi}_{ij}^d = 0.1$ (Scenario C).

W^+h^0 is the most relevant one.

Scenario D. In Fig. 5 we present plots for the BRs of the channels $t\bar{b}$, $c\bar{b}$, $t\bar{s}$, $\tau^+\nu_\tau$, W^+h^0 , W^+A^0 as a function of m_{H^+} . For $\tan\beta = 0.1$, we show in Fig. 5(a) that the dominant decay modes for the H^+ are: $c\bar{b}$ in the range $m_{H^+} < 175$ GeV, $t\bar{s}$ when $175 \text{ GeV} < m_{H^+} < 180$ GeV, $t\bar{b}$ for $180 \text{ GeV} < m_{H^+}$. For $\tan\beta = 1$, we show in Fig. 5(b) that the mode $\tau^+\nu_\tau$ is dominant in the range $m_{H^+} < 175$ GeV, whereas for $175 \text{ GeV} < m_{H^+} < 180$ GeV the relevant decay channel is $t\bar{s}$, whilst the mode $t\bar{b}$ dominates for $180 \text{ GeV} < m_{H^+} < 550$ GeV and the mode W^+A^0 does so when $550 \text{ GeV} < m_{H^+}$. For $\tan\beta = 15$, we observe in Fig. 5(c) that the relevant decay channels are: $\tau^+\nu_\tau$ in the range $m_{H^+} < 250$ GeV and W^+h^0 for $250 \text{ GeV} < m_{H^+}$. Finally, for $\tan\beta = 70$, see Fig. 5(d), we obtain that, when $m_{H^+} < 230$ GeV, the mode $\tau^+\nu_\tau$ becomes the most important one but, for $230 \text{ GeV} < m_{H^+} < 800$ GeV, the channel $t\bar{b}$ is the leading one, whereas, for $800 \text{ GeV} < m_{H^+}$, the mode W^+h^0 is the dominant one.

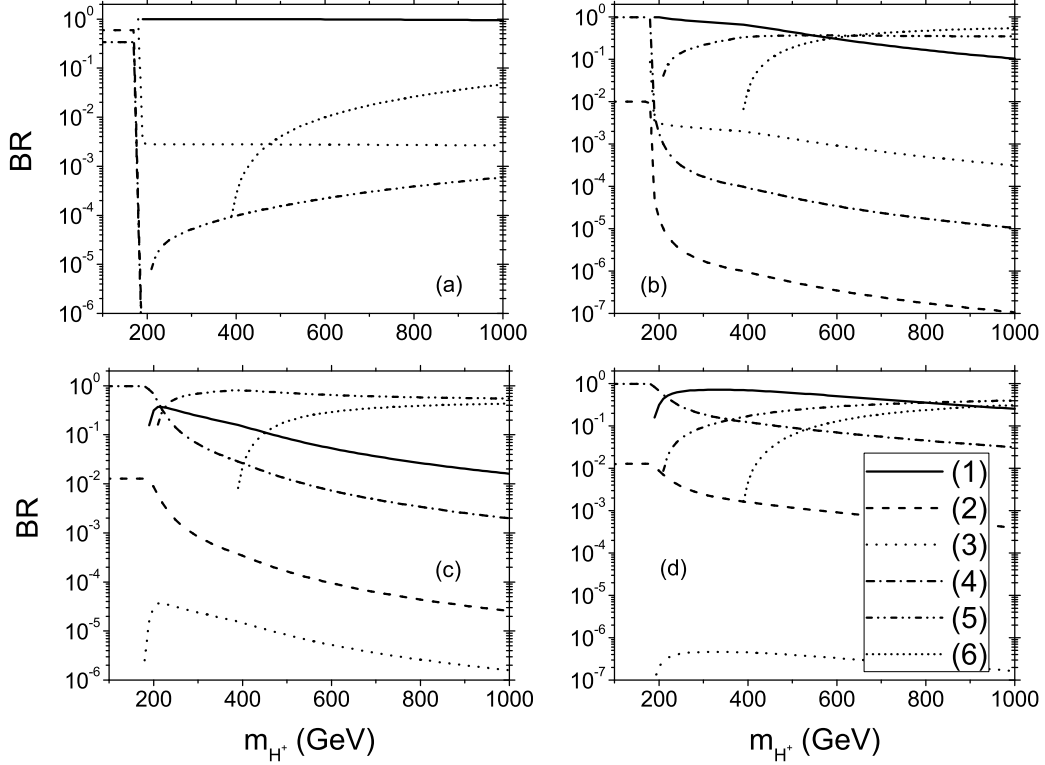


FIG. 5: The same as in Fig. 2, but taking $\tilde{\chi}_{ij}^u = 0.1$, $\tilde{\chi}_{ij}^d = 0.1$ (Scenario D).

In order to cover further the Higgs sector in our analysis, it is appropriate to also mention how the previous results change with m_{h^0} , m_{A^0} and α . Regarding the former two, clearly, the later the neutral Higgs boson mass the later the corresponding H^\pm decay channel will onset. Regarding the latter, we adopted two further choices, $\alpha = \beta$ and 0, in all scenarios previously studied. In general the behavior of the decay modes of the charged Higgs boson is similar to the cases presented above, except for the decay channel Wh^0 . For $\alpha = 0$, this mode has $\text{BR} < 10^{-3}$ when $\tan\beta$ is large. However, for $\tan\beta < 1$, it becomes the dominant one. In the case $\alpha = \beta$, the decay channel Wh^0 can be dominant with a BR that could be $O(1)$.

As a general lesson from this section, and distinctive features of our 2HDM-III, we can see that both decay modes W^+h^0 and $c\bar{b}$ become very relevant phenomenologically, effectively of $O(1)$ for some of the scenarios considered. Therefore, we want to study next the general behaviour of

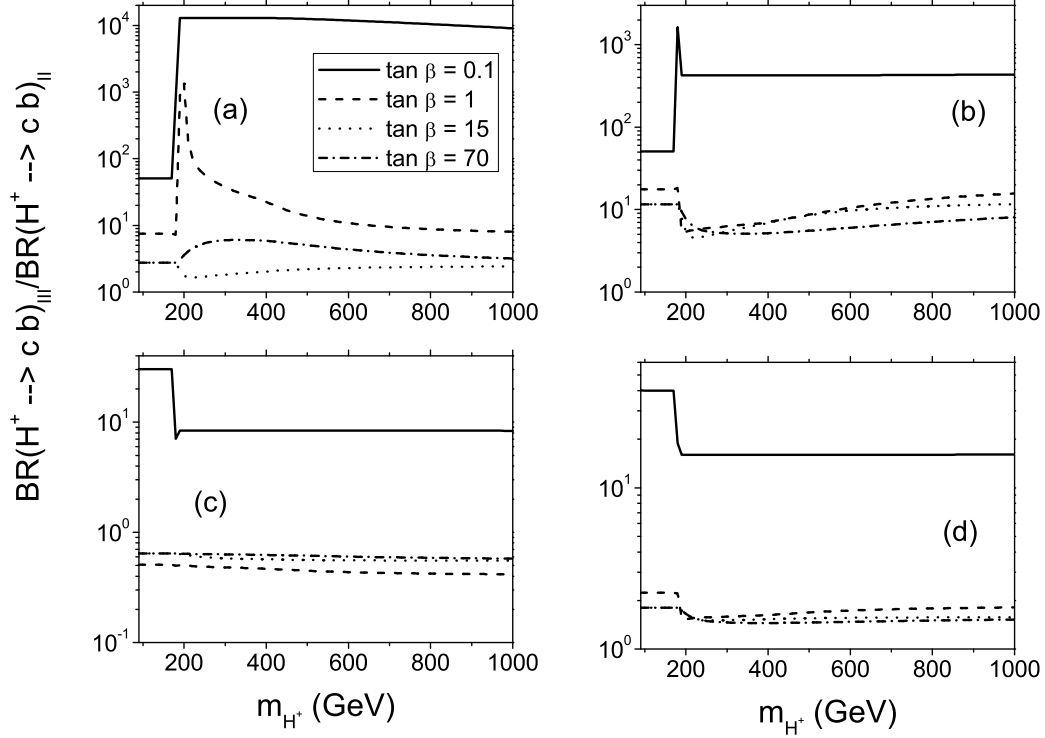


FIG. 6: The figure shows the $\text{BR}(H^+ \rightarrow c\bar{b})_{\text{III}}/\text{BR}(H^+ \rightarrow c\bar{b})_{\text{II}}$ vs. m_{H^+} , taking $\tan\beta = 0.1, 1, 15, 70$ for (a) $\tilde{\chi}_{ij}^{u,d} = 1$, (b) $\tilde{\chi}_{ij}^{u,d} = -1$, (c) $\tilde{\chi}_{ij}^{u,d} = 0.1$, (d) $\tilde{\chi}_{ij}^{u,d} = -0.1$.

these decay modes, in relation to the 2HDM-II case. In order to compare the 2HDM-III results with those in the 2HDM-II, we show in Fig. 6 the ratio $\text{BR}(H^+ \rightarrow c\bar{b})_{\text{III}}/\text{BR}(H^+ \rightarrow c\bar{b})_{\text{II}}$ vs. m_{H^+} , taking again $\tan\beta = 0.1, 1, 15, 70$, for: (a) $\tilde{\chi}_{ij}^{u,d} = 1$, (b) $\tilde{\chi}_{ij}^{u,d} = -1$, (c) $\tilde{\chi}_{ij}^{u,d} = 0.1$ and (d) $\tilde{\chi}_{ij}^{u,d} = -0.1$. We observe that the mode $c\bar{b}$ is important when $200 \text{ GeV} < m_{H^+} < 300 \text{ GeV}$ and for $0.1 \leq \tan\beta \leq 1$, taking $\tilde{\chi}_{ij}^{u,d} = 1$. Now, in Fig. 7, we present the behaviour of the ratio $\text{BR}(H^+ \rightarrow c\bar{b})_{\text{III}}/\text{BR}(H^+ \rightarrow c\bar{b})_{\text{II}}$ as a function of $\tilde{\chi}_{ij}^{u,d}$, for the cases: (a) $m_{H^+} = 150 \text{ GeV}$, (b) $m_{H^+} = 300 \text{ GeV}$, (c) $m_{H^+} = 450 \text{ GeV}$ and (d) $m_{H^+} = 600 \text{ GeV}$. Again, one can see that the largest enhancement arises when $m_{H^+} = 300 \text{ GeV}$ and $\tilde{\chi}_{ij}^{u,d} = 1$. Finally, specific to the 2HDM-III, we show in Fig. 8 the ratio $\text{BR}(H^+ \rightarrow W^+ h^0)_{\text{III}}/\text{BR}(H^+ \rightarrow c\bar{b})_{\text{III}}$ vs. m_{H^+} , taking $\tan\beta = 0.1, 1, 15, 70$, for: (a) $\tilde{\chi}_{ij}^{u,d} = 0.1$, (b) $\tilde{\chi}_{ij}^{u,d} = -0.1$, (c) $\tilde{\chi}_{ij}^{u,d} = 1$ and (d) $\tilde{\chi}_{ij}^{u,d} = 1$. We find that $\text{BR}(H^+ \rightarrow W^+ h^0)_{\text{III}}$ is much larger than $\text{BR}(H^+ \rightarrow c\bar{b})_{\text{III}}$ when $\tilde{\chi}_{ij}^{u,d} = 1$ and the mass of the charged Higgs boson is close to the upper limit obtained by unitarity conditions, which is about 800 GeV [26]. Thus, we find that the effect of the modified Higgs couplings typical of the 2HDM-III

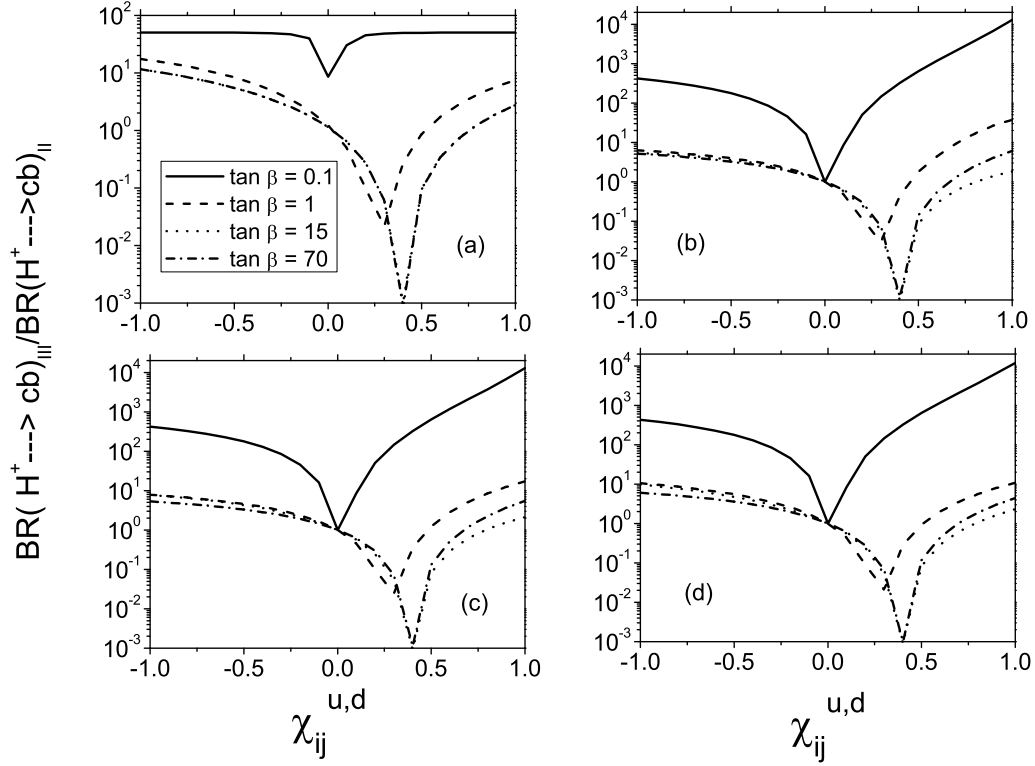


FIG. 7: The figure shows the $\text{BR}(H^+ \rightarrow c\bar{b})_{\text{III}}/\text{BR}(H^+ \rightarrow c\bar{b})_{\text{II}}$ vs. $\tilde{\chi}_{ij}^{u,d}$, taking $\tan\beta = 0.1, 1, 15, 70$ for (a) $m_{H^+} = 150$ GeV, (b) $m_{H^+} = 300$ GeV, (c) $m_{H^+} = 450$ GeV, (d) $m_{H^+} = 600$ GeV.

shows up clearly in the pattern of charged Higgs boson decays, which can be very different from the 2HDM-II case and thus enrich the possibilities to search for H^\pm states at current (Tevatron) and future (LHC, ILC/CLIC) machines.

IV. CHARGED HIGGS BOSON PRODUCTION AT LHC

The production of charged Higgs bosons at hadron colliders has been evaluated in early [21] (also for the Superconducting Super Collider, SSC) and more recent [22] (for the LHC) literature, mainly for the 2HDM-II and its SUSY realization (i.e., the MSSM). In these two scenarios, when kinematically allowed, the top quark decay channel $t \rightarrow bH^+$ is the dominant H^\pm production mechanism. Instead, above the threshold for such a decay, the dominant H^\pm production reaction

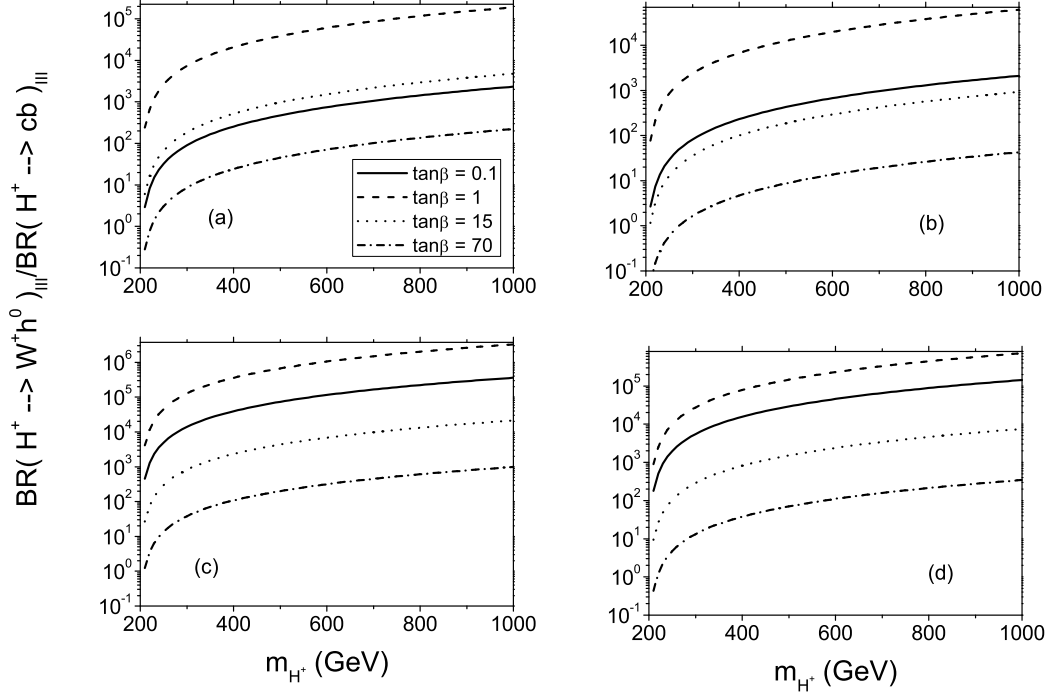


FIG. 8: The figure shows the $\text{BR}(H^+ \rightarrow W^+ h^0)_{\text{III}} / \text{BR}(H^+ \rightarrow c\bar{b})_{\text{III}}$ vs. m_{H^+} , taking $\tan \beta = 0.1, 1, 15, 70$ for (a) $\tilde{\chi}_{ij}^{u,d} = 0.1$, (b) $\tilde{\chi}_{ij}^{u,d} = -0.1$, (c) $\tilde{\chi}_{ij}^{u,d} = 1$, (d) $\tilde{\chi}_{ij}^{u,d} = -1$.

is gluon-gluon fusion into a 3-body final state, i.e., $gg \rightarrow tbH^{\pm 4}$. Both processes depend on the coupling $H^- t\bar{b}$ and are therefore sensitive to the modifications that arise in the 2HDM-III for this vertex. However, detection of the final state will depend on the charged Higgs boson decay mode, which could include a complicated final state, that could in turn be difficult to reconstruct. For these reasons, it is very important to look for other production channels, which may be easier to reconstruct. In this regard, the s -channel production of charged Higgs bosons, through the mechanism of $c\bar{b}$ -fusion, could help to make more viable the detection of several charged Higgs boson decay channels [27].

Here, we shall evaluate the predictions of the 2HDM-III for the $t \rightarrow bH^+$ (and sH^+) decay rate plus the $c\bar{b}$ - as well as the gg -fusion mechanisms (hereafter, referred to as ‘direct’ and ‘indirect’ H^{\pm} production, respectively).

⁴ In fact, these two mechanisms are intimately related, see below.

A. The decays $t \rightarrow H^+ b, H^+ s$

We shall discuss here the charged Higgs boson interactions with heavy quarks (t, b, c, s) and their implications for charged Higgs boson production through top quark decays. In order to study the top quark BRs, besides the SM decay mode $t \rightarrow bW^+$, we need to consider both decays $t \rightarrow bH^+$ and $t \rightarrow sH^+$, because these modes could both be important for several parameter configurations within our model. The decay width of these modes takes the following form:

$$\Gamma(t \rightarrow d_j H^+) = \frac{g^2}{128\pi m_W^2 m_t^3} \lambda^{1/2}(m_t^2, m_{H^+}^2, m_b^2) \times \left(\left[(m_t + m_b)^2 - m_{H^+}^2 \right] S_{3j}^2 + \left[(m_t + m_b)^2 - m_{H^+}^2 \right] P_{3j}^2 \right), \quad (12)$$

where λ is the usual kinematic factor $\lambda(a, b, c) = (a - b - c)^2 - 4bc$, $j = 2$ for the mode sH^+ and $j = 3$ for the mode bH^+ . Furthermore, we shall neglect the decay width for the light fermion generations. If one takes $\tilde{\chi}_{i,j} \rightarrow 0$, the formulae for the decay width reduce to the 2HDM-II case: see, e.g., [2].

We have explored several theoretically allowed regions within our scenario, which are constrained by using the bounds on the $\text{BR}(t \rightarrow bH^+)$. In the so-called “tauonic Higgs model” [23], the decay mode ($H^+ \rightarrow \tau^+ \nu_\tau$) dominates the charged Higgs boson decay width, and $\text{BR}(t \rightarrow bH^+)$ is constrained to be less than 0.4 at 95 % C.L. [23]. However, if no assumption is made on the charged Higgs boson decay, $\text{BR}(t \rightarrow bH^+)$ is constrained to be less than 0.91 at 95 % C.L. [23]. However, the combined LEP data exclude a charged Higgs boson with mass less than 79.3 GeV at 95 % C.L., a limit valid for an arbitrary $\text{BR}(H^+ \rightarrow \tau^+ \nu_\tau)$ [25]. Thus, in order to perform our analysis, we need to discuss all the charged Higgs boson decays following the steps of our previous paper [19]. In the present section, we take all charged Higgs boson decays relevant for masses below that of the top quark, thus including the modes $\tau^+ \nu_\tau, t\bar{s}, c\bar{b}, W^+ h^0, W^+ A^0$. As usual, we refer to our four benchmark scenarios.

Scenario A. Remember that this scenario was defined by taking $\tilde{\chi}_{ij}^u = 1$ and $\tilde{\chi}_{ij}^d = 1$, while for $\tan \beta$ we considered the values $\tan \beta = 0.1, 1, 15, 70$. In Fig. 9 we present plots of $\text{BR}(t \rightarrow bH^+)$ vs. m_H^+ and $\text{BR}(t \rightarrow sH^+)$ vs. m_{H^+} . We can observe that a charged Higgs boson within the mass range $80 \text{ GeV} < m_{H^+} < 170 \text{ GeV}$ and for $1 < \tan \beta < 70$ satisfies the constraint $\text{BR}(t \rightarrow bH^+) < 0.4$. Furthermore, from the plots of Fig. 2, we can see that in this scenario the dominant decay mode is into $\tau^+ \nu_\tau$ for $\tan \beta = 1, 15, 70$, therefore we fall within the scope of the tauonic Higgs model, so that $\text{BR}(t \rightarrow H^+ b) \leq 0.4$ applies. However, for the case $\tan \beta = 0.1$, the dominant decay of the charged Higgs boson is the mode $c\bar{b}$ and the mode $t \rightarrow bH^+$ satisfies the constraint $\text{BR}(t \rightarrow bH^+) < 0.9$

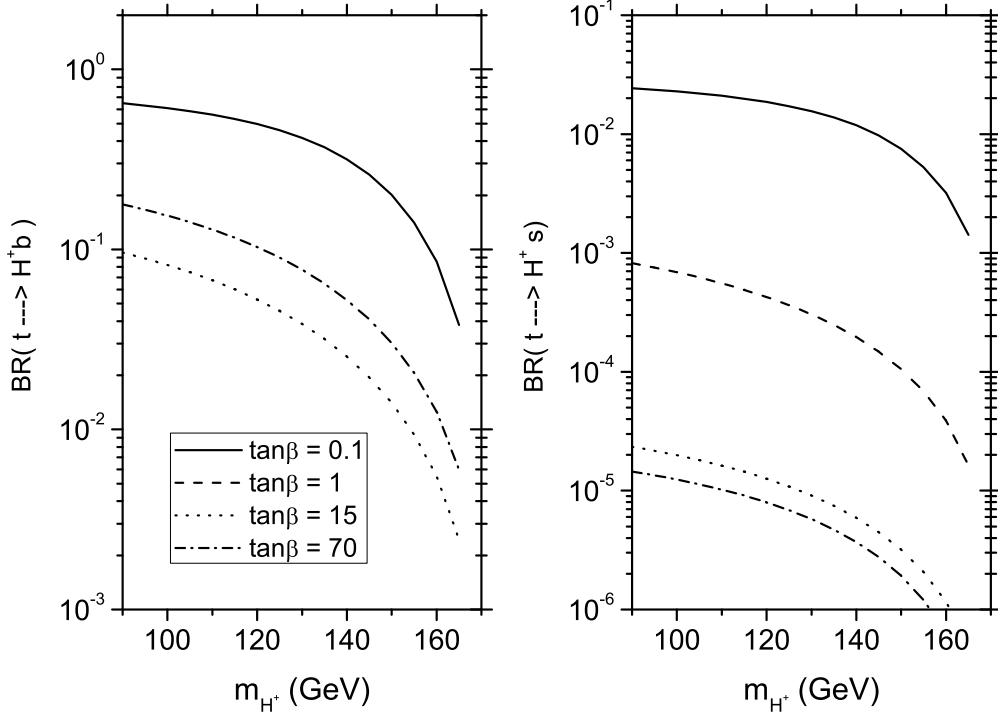


FIG. 9: It is plotted: the $BR(t \rightarrow b H^+)$ vs. m_{H^+} (left); the $BR(t \rightarrow s H^+)$ vs. m_{H^+} (right). Here is for Scenario A, obtained by taking $\tilde{\chi}_{ij}^u = 1$ and $\tilde{\chi}_{ij}^d = 1$, for $\tan\beta = 0.1$ (solid), 1 (dashes), 15 (dots) and 70 (dashes-dots).

in the range described above.

Scenario B. In Fig. 10 we present similar plots for the case $\tilde{\chi}_{ij}^u = 0.1$ and $\tilde{\chi}_{ij}^d = 1$, taking $\tan\beta = 0.1, 1, 15, 70$. We can observe that the mode $t \rightarrow b H^+$ satisfies the constraint $BR(t \rightarrow b H^+) < 0.4$ within the ranges $80 \text{ GeV} < m_{H^+} < 170 \text{ GeV}$ and $1 < \tan\beta < 70$. Thus, from Fig. 3, we can see that in this range the dominant decay mode is into $\tau^+ \nu_\tau$, therefore this setups also falls within the realm of the tauonic Higgs model, so that $BR(t \rightarrow H^+ b) \leq 0.4$ must hold in this scenario. For $\tan\beta = 0.1$, the dominant decay of the charged Higgs boson is $c\bar{b}$, thus the channel $t \rightarrow b H^+$ must satisfy the constraint $BR(t \rightarrow b H^+) < 0.9$, which is fulfilled in the range studied.

Scenario C. In Fig. 11 we present the corresponding plots for the case $\tilde{\chi}_{ij}^u = 1$ and $\tilde{\chi}_{ij}^d = 0.1$, taking again $\tan\beta = 0.1, 1, 15, 70$. We can observe that the mode $t \rightarrow b H^+$ satisfies the constraint $BR(t \rightarrow b H^+) < 0.4$ in the range $80 \text{ GeV} < m_{H^+} < 170 \text{ GeV}$ and $1 < \tan\beta < 70$. Similarly, as in scenario A, for $\tan\beta = 0.1$ the dominant decay of the charged Higgs boson is the mode $c\bar{b}$, thus

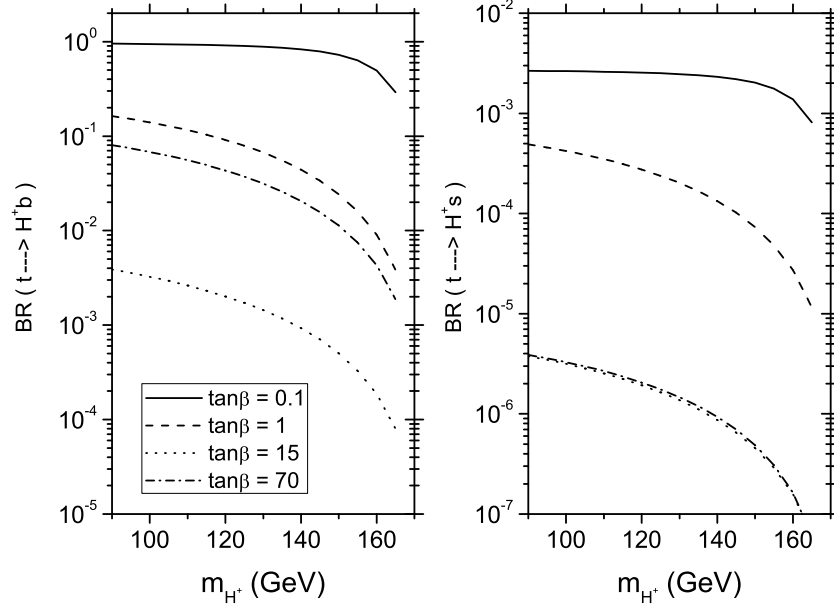


FIG. 10: The same as in Fig. 9 but taking $\tilde{\chi}_{ij}^u = 0.1$ and $\tilde{\chi}_{ij}^d = 1$ (Scenario B).

the mode $t \rightarrow b H^+$ must satisfies the constraint $\text{BR}(t \rightarrow b H^+) < 0.9$, indeed satisfied in the range analyzed here.

Scenario D. Recall that this was defined by taking $\tilde{\chi}_{ij}^u = 0.1$ and $\tilde{\chi}_{ij}^d = 0.1$. In Fig. 12 we present the usual plots of the $\text{BR}(t \rightarrow b H^+)$ and $\text{BR}(t \rightarrow b H^+) \text{ vs. } m_{H^+}$. One can see that, for charged Higgs boson masses within the range $80 \text{ GeV} < m_{H^+} < 170 \text{ GeV}$ and $1 < \tan \beta < 70$, the model fulfills the constraint $\text{BR}(t \rightarrow b H^+) < 0.4$. Furthermore, for $\tan \beta = 0.1$, the dominant decay of the charged Higgs boson is the mode $c\bar{b}$, thus the mode $t \rightarrow b H^+$ satisfies the constraint $\text{BR}(t \rightarrow b H^+) < 0.9$ in the range studied.

In short, as bottomline of these exercises, we have identified regions of the 2HDM-III parameter space where a charged Higgs mass below $m_t - m_b$ has not been excluded by Tevatron. Therefore, the LHC is best positioned in order to probe charged Higgs bosons with such masses.

B. Direct production of charged Higgs bosons at the LHC

The $H^\pm \bar{q}q'$ vertex with large flavor mixing coupling, that arises in the 2HDM-III, enables the possibility of studying the production of charged Higgs boson via the s -channel production mechanism, $c\bar{b} \rightarrow H^+ + \text{c.c.}$ This process was discussed first by Ref. [27], both within topcolor

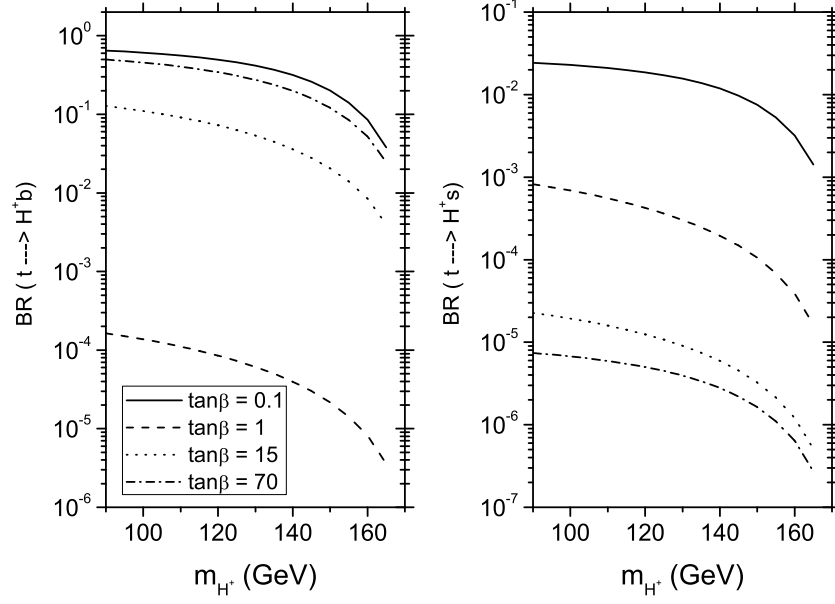


FIG. 11: The same as in Fig. 9 but taking $\tilde{\chi}_{ij}^u = 1$ and $\tilde{\chi}_{ij}^d = 0.1$ (Scenario C).

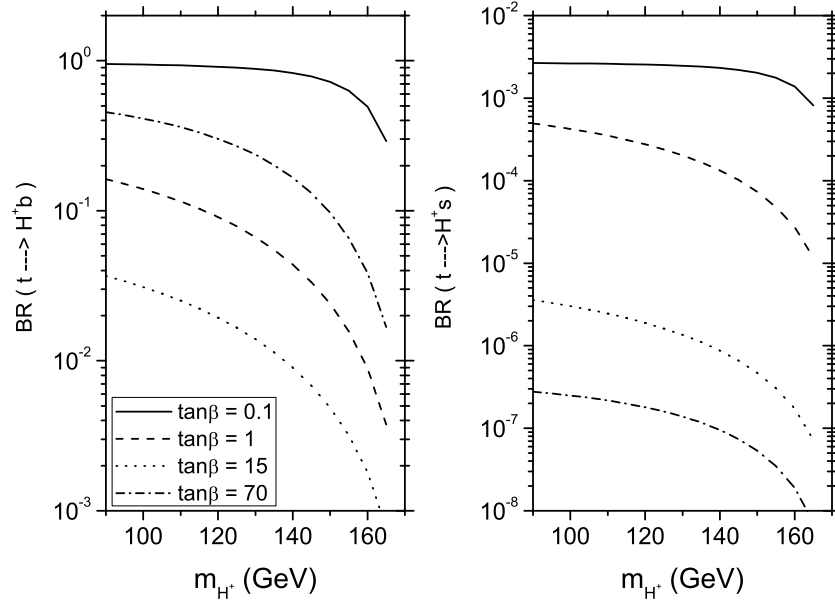


FIG. 12: The same as in Fig. 9 but taking $\tilde{\chi}_{ij}^u = 0.1$ and $\tilde{\chi}_{ij}^d = 0.1$ (Scenario D).

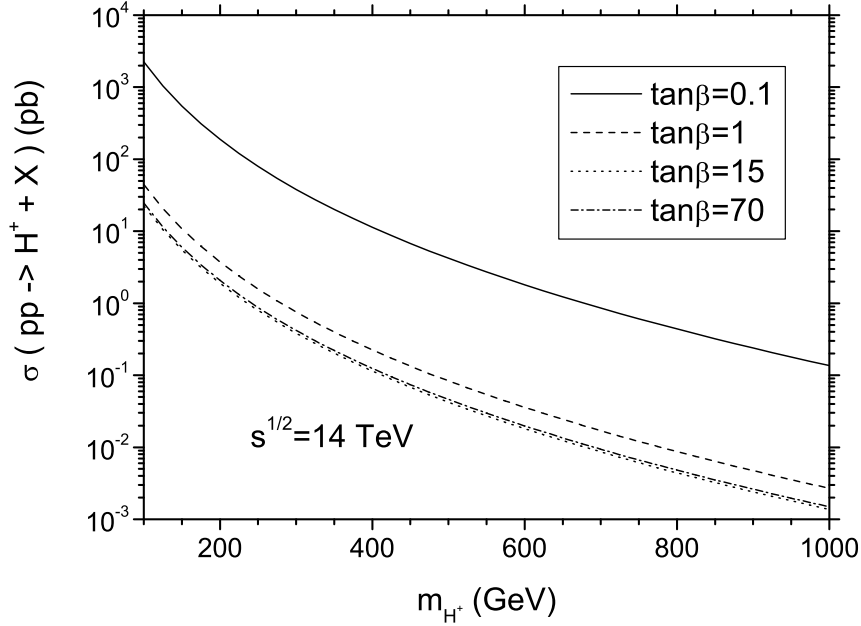


FIG. 13: The figure shows the total cross section rates of process $h_1 h_2 (c\bar{b}) \rightarrow H^+ X$ as a function of m_{H^+} in the 2HDM-III at LHC energies ($\sqrt{s} = 14$ TeV), by taking $\tilde{\chi}_{l3}^d = 1$ and $\tilde{\chi}_{2l}^u = 1$ ($l = 1, 2, 3$). The lines correspond to: $\tan \beta = 0.1$, $\tan \beta = 1$, $\tan \beta = 15$, $\tan \beta = 70$.

models and a simplified version of the 2HDM-III. Then the SUSY case was discussed in [39] and [40]. Here we perform a detailed study of this mechanism within the 2HDM-III, paying special attention to the effects induced by the assumed Yukawa texture on the charged Higgs boson couplings. Defining the $H^\pm \bar{q} q'$ coupling here as $C_L \frac{1-\gamma_5}{2} + C_R \frac{1+\gamma_5}{2}$, we can express the total cross section for H^+ direct production at hadron colliders as [27]

$$\sigma(h_1 h_2 (c\bar{b}) \rightarrow H^+ X) = \frac{\pi}{12s} (|C_L|^2 + |C_R|^2) I_{c,\bar{b}}^{h_1, h_2}, \quad (13)$$

where

$$I_{c,\bar{b}}^{h_1, h_2} = \int_\tau^1 \frac{dx}{x} [f_c^{h_1}(x, \tilde{Q}^2) f_{\bar{b}}^{h_2}(\tau/x, \tilde{Q}^2) + f_{\bar{b}}^{h_1}(x, \tilde{Q}^2) f_c^{h_2}(\tau/x, \tilde{Q}^2)] \quad (14)$$

and $\tau = m_{H^\pm}^2/s$. The Parton Distribution Functions (PDFs) $f_q^{h_i}(x, \tilde{Q}^2)$ used here are from [41], with scale choice $\tilde{Q}^2 = m_{H^+}^2$.

From Eq. (6) we see that, for the case of the 2HDM-III, C_L and C_R entering the subprocess $c\bar{b} \rightarrow H^+$ are given by

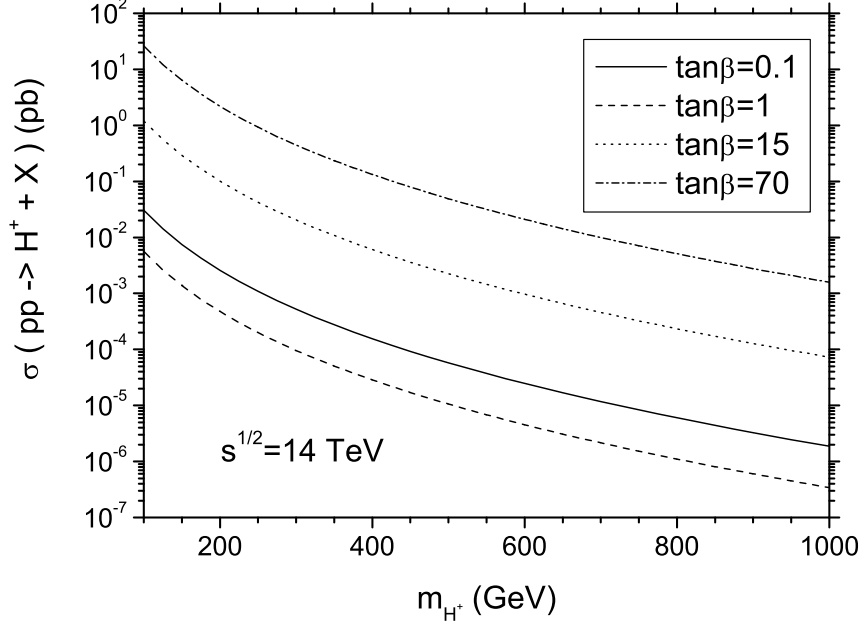


FIG. 14: The figure shows the total cross section rates of process $h_1 h_2 (c\bar{b}) \rightarrow H^+ X$ as a function of m_{H^+} in the 2HDM-II at LHC energies ($\sqrt{s} = 14$ TeV), by taking $(V_{\text{CKM}})_{23} = 4.16 \times 10^{-2}$ and $(V_{\text{CKM}})_{33} \approx 1$. The lines correspond to: $\tan \beta = 0.1$, $\tan \beta = 1$, $\tan \beta = 15$, $\tan \beta = 70$.

$$C_L \equiv C_L^{\text{III}} = -\frac{ig}{\sqrt{2}M_W} \sum_{l=1}^3 \left[\cot \beta m_c \delta_{2l} - \frac{\csc \beta}{\sqrt{2}} \sqrt{m_c m_{u_l}} \tilde{\chi}_{2l}^u \right] (V_{\text{CKM}})_{l3}, \quad (15)$$

and

$$C_R \equiv C_R^{\text{III}} = -\frac{ig}{\sqrt{2}M_W} \sum_{l=1}^3 \left[\tan \beta m_{d_l} \delta_{l3} - \frac{\sec \beta}{\sqrt{2}} \sqrt{m_{d_l} m_{d_3}} \tilde{\chi}_{l3}^d \right] (V_{\text{CKM}})_{2l}. \quad (16)$$

We notice here that Eqs. (15) and (16) reduce to the case of the 2HDM-II if one takes

$$C_L \equiv C_L^{\text{II}} = -\frac{ig}{\sqrt{2}M_W} \cot \beta m_c (V_{\text{CKM}})_{23} \quad (17)$$

and

$$C_R \equiv C_R^{\text{II}} = -\frac{ig}{\sqrt{2}M_W} \tan \beta m_b (V_{\text{CKM}})_{23}. \quad (18)$$

In Fig. 13, we present plots for the total cross section rates of process $h_1 h_2 (c\bar{b}) \rightarrow H^+ X$ as a function of m_{H^+} in the framework of the 2HDM-III, by taking $\tilde{\chi}_{l3}^d = 1$ and $\tilde{\chi}_{2l}^u = 1$ ($l = 1, 2, 3$),

at LHC energies ($\sqrt{s} = 14$ TeV), for the cases: (a) $\tan\beta = 0.1$, (b) $\tan\beta = 1$, (c) $\tan\beta = 15$, (d) $\tan\beta = 70$. The sum over l is performed over all the three quark families and we take for the quark masses: $m_u = 2.55$ MeV, $m_d = 5.04$ MeV, $m_c = 1.27$ GeV, $m_s = 104$ MeV, $m_b = 4.20$ GeV, and $m_t = 171.2$ GeV [25]. We have checked numerically that the term proportional to $\frac{1}{2} \csc^2\beta m_c m_t |\tilde{\chi}_{23}^u (V_{\text{CKM}})_{33}|^2$ provides the most important contribution to the cross section rates and dominates by far for $\tilde{\chi}_{23}^u \approx 1$. On the other hand, the expected integrated luminosity at LHC is of the order 10^5 pb^{-1} and given that $\sigma \gtrsim 10^{-5} \text{ pb}$ even for $\tan\beta = 70$ and $m_{H^\pm} \lesssim 600$ GeV, we can conclude that, in the context of the 2HDM-III, it is likely that a charged Higgs boson could be observed at LHC energies by exploiting direct production.

In Fig. 14, we present results for the total cross section rates of process $h_1 h_2 (c\bar{b}) \rightarrow H^\pm X$ as a function of m_{H^\pm} in the 2HDM-II at LHC energies ($\sqrt{s} = 14$ TeV), by taking $(V_{\text{CKM}})_{23} = 4.16 \times 10^{-2}$ and $(V_{\text{CKM}})_{33} \approx 1$, for the cases: (a) $\tan\beta = 0.1$, (b) $\tan\beta = 1$, (c) $\tan\beta = 15$, and (d) $\tan\beta = 70$. As we have already said, the expected integrated luminosity at LHC is of the order 10^5 pb^{-1} , hence we also conclude from this figure that in the framework of the 2HDM-II we obtain production rates for the charged Higgs boson via $c\bar{b}$ -fusion that may be detectable at LHC energies.

C. Indirect production of charged Higgs bosons at the LHC

We have found that, in some of the 2HDM-III scenarios envisaged here, light charged Higgs bosons could exist that have not been excluded by current experimental bounds, chiefly from LEP2 and Tevatron. Their discovery potential should therefore be studied in view of the upcoming LHC and we shall then turn our attention now to presenting the corresponding hadro-production cross sections via an indirect channel, i.e., other than as secondary products in (anti)top quark decays and via $c\bar{b}$ -fusion, considered previously.

As dealt with so far, if the charged Higgs boson mass m_{H^\pm} satisfies $m_{H^\pm} < m_t - m_b$, where m_t is the top quark mass and m_b the bottom quark mass, H^\pm particles could be produced in the decay of on-shell (i.e., $\Gamma_t \rightarrow 0$) top (anti-)quarks $t \rightarrow bH^+$ and the c.c. process, the latter being in turn produced in pairs via $q\bar{q}$ annihilation and gg fusion. We denote such a H^\pm production channel as $q\bar{q}, gg \rightarrow t\bar{t} \rightarrow t\bar{b}H^- + \text{c.c.}$ (i.e., if due to (anti-)top decays) whilst we use the notation $q\bar{q}, gg \rightarrow t\bar{b}H^- + \text{c.c.}$ to signify when further production diagrams are included⁵. In fact, owing to the

⁵ Altogether, they represent the full gauge invariant set of Feynman graphs pertaining to the $2 \rightarrow 3$ body process with a $t\bar{b}H_i^- + \text{c.c.}$ final state: two for the case of $q\bar{q}$ annihilation and eight for gluon-gluon fusion, see, e.g., Eq. (1.1) of [42].

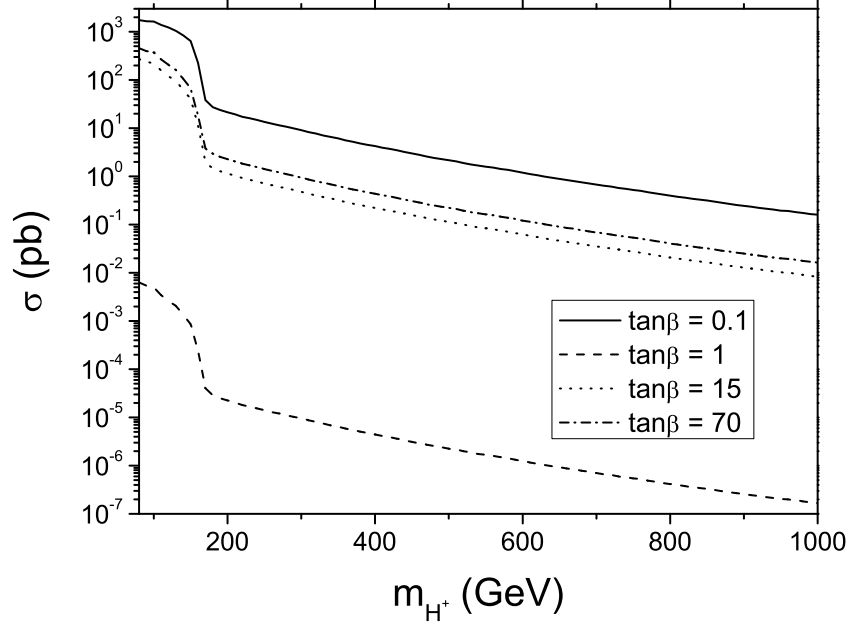


FIG. 15: The figure shows the cross sections of H^+ production at the LHC through the channel $q\bar{q}, gg \rightarrow t\bar{b}H^- + \text{c.c.}$ in Scenario A ($\tilde{\chi}_{ij}^u = 1$ and $\tilde{\chi}_{ij}^d = 1$) and for $\tan\beta = 0.1, 1, 15, 70$.

large top decay width ($\Gamma_t \geq 1.5$ GeV) and due to the additional diagrams which do not proceed via direct $t\bar{t}$ production but yield the same final state $t\bar{b}H^- + \text{c.c.}$ [43, 44, 45], charged Higgs bosons could also be produced at and beyond the kinematic top decay threshold. The importance of these effects in the so-called ‘threshold’ or ‘transition’ region ($m_{H^\pm} \approx m_t$) was emphasized in various Les Houches proceedings [46, 47] as well as in Refs. [42, 48, 49, 50], so that the calculations of Refs. [43, 44] (based on the appropriate $q\bar{q}, gg \rightarrow t\bar{b}H^\pm$ description) are now implemented in HERWIG [51, 52, 53, 54] and PYTHIA [55, 56]. A comparison between the two generators was carried out in Ref. [48]. For any realistic simulation of H^\pm production with $m_{H^\pm} \gtrsim m_t$, as can well be the case here, the use of either of these two implementations is of paramount importance.

Here, we use HERWIG version 6.510 in default configuration, by onsetting the subprocess `IPROC = 3839`, wherein we have overwritten the default MSSM/2HDM couplings and masses with those pertaining to the 2HDM-III: see Eqs. (7)–(8). The production cross sections are found in Figs. 15–18 for our usual scenarios: A ($\tilde{\chi}_{ij}^u = 1$ and $\tilde{\chi}_{ij}^d = 1$), B ($\tilde{\chi}_{ij}^u = 1$ and $\tilde{\chi}_{ij}^d = 0.1$), C ($\tilde{\chi}_{ij}^u = 0.1$ and $\tilde{\chi}_{ij}^d = 1$) and D ($\tilde{\chi}_{ij}^u = 0.1$ and $\tilde{\chi}_{ij}^d = 0.1$). As usual, we adopt our four choices of $\tan\beta$.

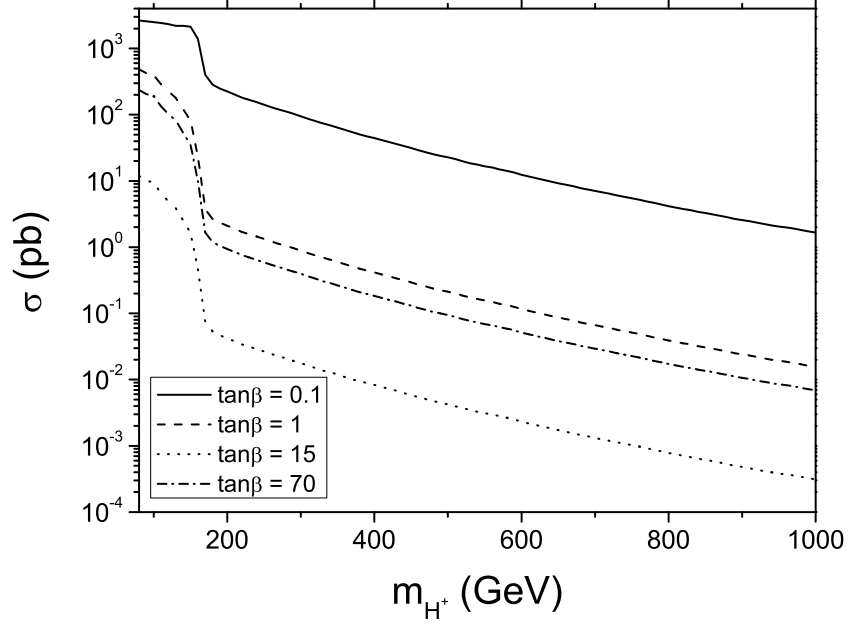


FIG. 16: The same as in Fig. 15 but taking $\tilde{\chi}_{ij}^u = 1$ and $\tilde{\chi}_{ij}^d = 0.1$ (Scenario B).

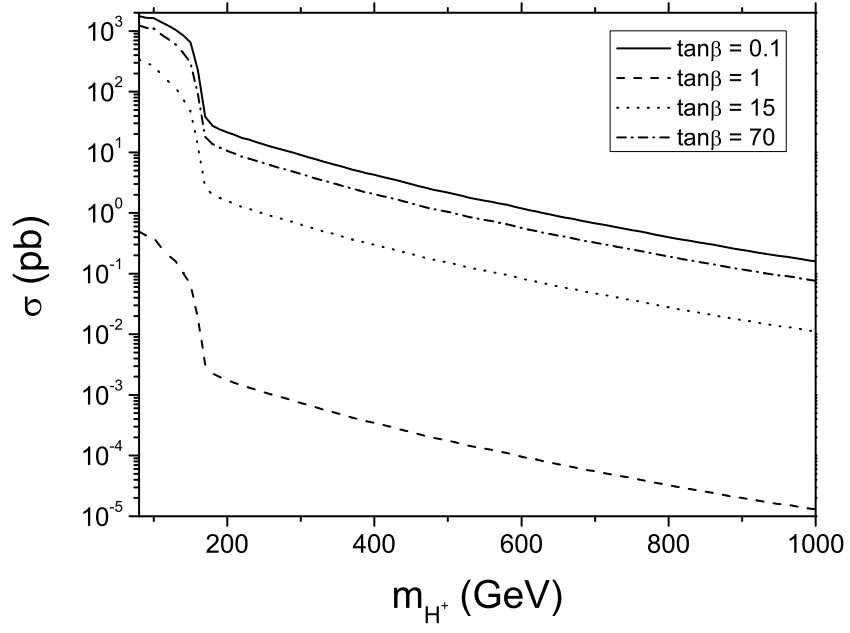


FIG. 17: The same as in Fig. 15 but taking $\tilde{\chi}_{ij}^u = 0.1$ and $\tilde{\chi}_{ij}^d = 1$ (Scenario C).

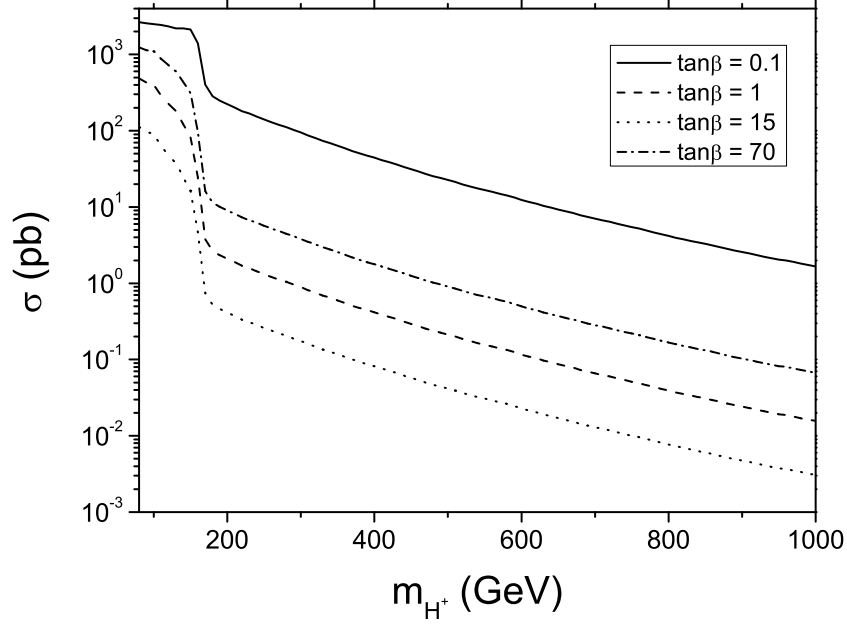


FIG. 18: The same as in Fig. 15 but taking $\tilde{\chi}_{ij}^u = 0.1$ and $\tilde{\chi}_{ij}^d = 0.1$ (Scenario D).

Altogether, by comparing the $q\bar{q}, gg \rightarrow t\bar{b}H_i^- + \text{c.c.}$ cross sections herein with, e.g., those of the MSSM in [6] or the 2HDM in [49, 57], it is clear that the 2HDM-III rates can be very large and thus the discovery potential in ATLAS and CMS can be substantial, particularly for a very light H^\pm , which may pertain to our 2HDM-III but not the MSSM or 2HDM-II. However, it is only by combining the production rates of this section with the decay ones of the previous ones that actual event numbers at the LHC can be predicted.

V. EVENT RATES OF CHARGED HIGGS BOSONS AT THE LHC

To illustrate the type of charged Higgs signatures that have the potential to be detectable at the LHC in the 2HDM-III, we show in Tabs. I and II the event rates of charged Higgs boson through the channels $q\bar{q}, gg \rightarrow t\bar{b}H_i^- + \text{c.c.}$ and $c\bar{b} \rightarrow H^+ + \text{c.c.}$, alongside the corresponding production cross sections (σ 's) and relevant BRs, for a combination of masses, $\tan\beta$ and specific 2HDM-III parameters amongst those used in the previous sections (assuming $m_{h^0} = 120$ GeV, $m_{A^0} = 300$ GeV and the mixing angle at $\alpha = \pi/2$ throughout). In particular, we focus on those cases where the charged Higgs boson mass is above the threshold for $t \rightarrow bH^+$, for two reasons. On the one

hand, the scope of the LHC in accessing $t \rightarrow bH^+$ decays has been established in a rather model independent way. On the other hand, we have dealt at length with the corresponding BRs in section III. (As default, we also assume an integrated luminosity of 10^5 pb^{-1} .)

To illustrate these results, let us comment on one case within each scenario. From Table I, we can see that for Scenario A, with $(\tilde{\chi}_{ij}^u = 1, \tilde{\chi}_{ij}^d = 1)$ and $\tan \beta = 15$, we have that the H^\pm is heavier than $m_t - m_b$, as we take a mass $m_{H^+} = 400$, thus precluding top decay contributions, so that in this case $\sigma(pp \rightarrow t\bar{b}H^+) \approx 2.2 \times 10^{-1} \text{ pb}$, while the dominant decays are $H^+ \rightarrow t\bar{b}, \tau^+\nu_\tau W^+h^0, W^+A^0$ which give a number of events of 7040, 46, 13860, 374, respectively. In this case the most promising signal is $H^+ \rightarrow W^+h^0$. However, when $\tan \beta = 70$ we have that all event rates increase substantially. Here, the signal $H^+ \rightarrow W^+h^0$ is still the most important with an event rate of 15480.

Then, for Scenario B ($\tilde{\chi}_{ij}^u = 0.1, \tilde{\chi}_{ij}^d = 1$), we have that H^\pm is again above the threshold for $t \rightarrow H^\pm b$. So, for the declared values of the relevant parameters, we take a charged Higgs boson mass $m_{H^+} = 600$ for $\tan \beta = 1$ and $\tan \beta = 70$, respectively. In such a case the decay $H^+ \rightarrow W^+h^0$ can reach significant numbers for the LHC. We obtain a number of events of 3960 and 2703, respectively. The other decay that has a large BR is $H^+ \rightarrow W^+A^0$, and in these cases the number of events ranges over 1200–3500.

Next, we discuss the Scenario C ($\tilde{\chi}_{ij}^u = 1, \tilde{\chi}_{ij}^d = 0.1$) for $\tan \beta = 15$. Here, we obtain that the signals $H^+ \rightarrow t\bar{b}$ and W^+h^0 are the most relevant ones, with a number of events about 34560 and 26240, respectively.

Finally, for scenario D ($\tilde{\chi}_{ij}^u = 0.11, \tilde{\chi}_{ij}^d = 0.1$) the dominant decays are $H^+ \rightarrow t\bar{b}, \tau^+\nu_\tau$ and W^+h^0 , which give a spectacular number of events: 269800, 68400 and 34200, respectively. Here, we have set $\tan \beta = 70$.

All these rates correspond to the case of indirect production. The contribution due to direct production is in fact subleading, especially at large m_{H^\pm} values. Nonetheless, in some benchmark cases, they could represent a sizable addition to the signal event rates. This is especially the case for Scenario A with $\tan \beta = 15$ or 70 and Scenario C with $\tan \beta = 15$. In general though, also considering the absence of an accompanying trigger alongside the H^\pm , *i.e.* for instance a top quark produced in $gb \rightarrow H^- t$ could help to identify the signal. Thus, we expect that the impact of $c\bar{b}$ -fusion at the LHC will be more marginal than that of gg -fusion for large Higgs masses, in fact, at times even smaller than the contribution from $q\bar{q}$ -annihilation.

TABLE I: Summary of LHC event rates for some parameter combinations within Scenarios A, B, C, D with for an integrated luminosity of 10^5 pb^{-1} , for several different signatures, through the channel $q\bar{q}, gg \rightarrow \bar{t}bH^+ + \text{c.c.}$

$(\tilde{\chi}_{ij}^u, \tilde{\chi}_{ij}^d)$	$\tan \beta$	m_{H^+} in GeV	$\sigma(pp \rightarrow H^+ \bar{t}b)$ in pb	Relevant BRs	Nr. Events
(1,1)	15	400	2.23×10^{-1}	$\text{BR}(H^+ \rightarrow t\bar{b}) \approx 3.2 \times 10^{-1}$ $\text{BR}(H^+ \rightarrow \tau^+ \nu_\tau^0) \approx 2.1 \times 10^{-3}$ $\text{BR}(H^+ \rightarrow W^+ h^0) \approx 6.3 \times 10^{-1}$ $\text{BR}(H_2^+ \rightarrow W^+ A^0) \approx 1.7 \times 10^{-2}$	7040 46 13860 374
(1,1)	70	400	4.3×10^{-1}	$\text{BR}(H^+ \rightarrow t\bar{b}) \approx 3.5 \times 10^{-1}$ $\text{BR}(H^+ \rightarrow c\bar{b}) \approx 1.4 \times 10^{-2}$ $\text{BR}(H^+ \rightarrow \tau^+ \nu_\tau) \approx 2.5 \times 10^{-1}$ $\text{BR}(H^+ \rightarrow W^+ h^0) \approx 3.6 \times 10^{-1}$	15050 602 10750 15480
(0.1,1)	1	600	1.1×10^{-1}	$\text{BR}(H^+ \rightarrow t\bar{b}) \approx 3 \times 10^{-1}$ $\text{BR}(H^+ \rightarrow t\bar{s}) \approx 9.1 \times 10^{-4}$ $\text{BR}(H^+ \rightarrow W^+ h^0) \approx 3.6 \times 10^{-1}$ $\text{BR}(H^+ \rightarrow W^+ A^0) \approx 3.2 \times 10^{-1}$	3300 10 3960 3520
(0.1,1)	70	600	5.1×10^{-2}	$\text{BR}(H^+ \rightarrow \tau^+ \nu_\tau) \approx 1.2 \times 10^{-1}$ $\text{BR}(H^+ \rightarrow t\bar{b}) \approx 9.4 \times 10^{-2}$ $\text{BR}(H^+ \rightarrow W^+ h^0) \approx 5.3 \times 10^{-1}$ $\text{BR}(H^+ \rightarrow W^+ A^0) \approx 2.3 \times 10^{-1}$	612 470 2703 1173
(1,0.1)	15	300	6.4×10^{-1}	$\text{BR}(H^+ \rightarrow t\bar{b}) \approx 5.4 \times 10^{-1}$ $\text{BR}(H^+ \rightarrow c\bar{b}) \approx 5 \times 10^{-4}$ $\text{BR}(H^+ \rightarrow \tau^+ \nu_\tau) \approx 3.9 \times 10^{-2}$ $\text{BR}(H^+ \rightarrow W^+ h^0) \approx 4.1 \times 10^{-1}$	34560 32 2535 26240
(0.1,0.1)	70	300	3.8	$\text{BR}(H^+ \rightarrow \tau^+ \nu_\tau) \approx 1.8 \times 10^{-1}$ $\text{BR}(H^+ \rightarrow t\bar{b}) \approx 7.1 \times 10^{-1}$ $\text{BR}(H^+ \rightarrow c\bar{b}) \approx 2.4 \times 10^{-3}$ $\text{BR}(H^+ \rightarrow W^+ h^0) \approx 9 \times 10^{-2}$	68400 269800 912 34200

VI. CONCLUSIONS

We have discussed the implications of assuming a four-zero Yukawa texture for the properties of the charged Higgs boson, within the context of a 2HDM-III. In particular, we have presented a detailed discussion of the charged Higgs boson couplings to heavy fermions and the resulting pattern for its decays. The latter clearly reflect the different coupling structure of the 2HDM-III, e.g., with respect to the 2HDM-II, so that one has at disposal more possibilities to search for H^\pm states at current and future colliders, ideally enabling one to distinguish between different Higgs models of EWSB. We have then concentrated our analysis to the case of the LHC and showed that the production rates of charged Higgs bosons at the LHC is sensitive to the modifications of the Higgs boson couplings. We have done so by evaluating 2HDM-III effects on the top decay

TABLE II: Summary of LHC event rates for some parameter combinations within Scenarios A, B, C, D with for an integrated luminosity of 10^5 pb^{-1} , for several different signatures, through the channel $c\bar{b} \rightarrow H^+ + \text{c.c.}$

$(\tilde{\chi}_{ij}^u, \tilde{\chi}_{ij}^d)$	$\tan \beta$	m_{H^+} in GeV	$\sigma(pp \rightarrow H^+ + X)$ in pb	Relevant BRs	Nr. Events
(1,1)	15	400	1.14×10^{-1}	$\text{BR}(H^+ \rightarrow t\bar{b}) \approx 3.2 \times 10^{-1}$	3648
				$\text{BR}(H^+ \rightarrow \tau^+ \nu_\tau^0) \approx 2.1 \times 10^{-3}$	24
				$\text{BR}(H^+ \rightarrow W^+ h^0) \approx 6.3 \times 10^{-1}$	7182
				$\text{BR}(H_2^+ \rightarrow W^+ A^0) \approx 1.7 \times 10^{-2}$	194
(1,1)	70	400	1.25×10^{-1}	$\text{BR}(H^+ \rightarrow t\bar{b}) \approx 3.5 \times 10^{-1}$	4375
				$\text{BR}(H^+ \rightarrow c\bar{b}) \approx 1.4 \times 10^{-2}$	175
				$\text{BR}(H^+ \rightarrow \tau^+ \nu_\tau) \approx 2.5 \times 10^{-1}$	3125
				$\text{BR}(H^+ \rightarrow W^+ h^0) \approx 3.6 \times 10^{-1}$	4500
(0.1,1)	1	600	3.41×10^{-4}	$\text{BR}(H^+ \rightarrow t\bar{b}) \approx 3 \times 10^{-1}$	10
				$\text{BR}(H^+ \rightarrow t\bar{s}) \approx 9.1 \times 10^{-4}$	0
				$\text{BR}(H^+ \rightarrow W^+ h^0) \approx 3.6 \times 10^{-1}$	12
				$\text{BR}(H^+ \rightarrow W^+ A^0) \approx 3.2 \times 10^{-1}$	11
(0.1,1)	70	600	1.98×10^{-3}	$\text{BR}(H^+ \rightarrow \tau^+ \nu_\tau) \approx 1.2 \times 10^{-1}$	24
				$\text{BR}(H^+ \rightarrow t\bar{b}) \approx 9.4 \times 10^{-2}$	19
				$\text{BR}(H^+ \rightarrow W^+ h^0) \approx 5.3 \times 10^{-1}$	105
				$\text{BR}(H^+ \rightarrow W^+ A^0) \approx 2.3 \times 10^{-1}$	45
(1,0.1)	15	300	3.99×10^{-1}	$\text{BR}(H^+ \rightarrow t\bar{b}) \approx 5.4 \times 10^{-1}$	21546
				$\text{BR}(H^+ \rightarrow c\bar{b}) \approx 5 \times 10^{-4}$	20
				$\text{BR}(H^+ \rightarrow \tau^+ \nu_\tau) \approx 3.9 \times 10^{-2}$	1556
				$\text{BR}(H^+ \rightarrow W^+ h^0) \approx 4.1 \times 10^{-1}$	16359
(0.1,0.1)	70	300	3.88×10^{-1}	$\text{BR}(H^+ \rightarrow \tau^+ \nu_\tau) \approx 1.8 \times 10^{-1}$	6984
				$\text{BR}(H^+ \rightarrow t\bar{b}) \approx 7.1 \times 10^{-1}$	27548
				$\text{BR}(H^+ \rightarrow c\bar{b}) \approx 2.4 \times 10^{-3}$	93
				$\text{BR}(H^+ \rightarrow W^+ h^0) \approx 9 \times 10^{-2}$	3492

$t \rightarrow bH^+$ as well as in the s -channel production of H^\pm through $c\bar{b}$ -fusion and the multibody final state induced by gg -fusion and $q\bar{q}$ -annihilation. Finally, we have determined the number of events for the most promising LHC signatures of a H^\pm belonging to a 2HDM-III, for both $c\bar{b} \rightarrow H^+ + \text{c.c.}$ and $q\bar{q} \rightarrow \bar{t}bH^+ + \text{c.c.}$ scatterings (the latter affording larger rates than the former). Armed with these results, we are now in a position to carry out a detailed study of signal and background rates, in order to determine the precise detectability level of each signature. However, this is beyond the scope of present work and will be the subject of a future publication.

Acknowledgements

This work was supported in part by CONACyT and SNI (México). J.H-S. thanks in particular CONACyT (México) for the grant J50027-F and SEP (México) by the grant PROMEP/103.5/08/1640. R.N-P. acknowledges the Institute of Physics BUAP for a warm hospitality and also financial support by CONACyT through the program *Apoyo Complementario para la Consolidación Institucional de Grupos de Investigación (Retención)*.

-
- [1] S. L. Glashow, Nucl. Phys. **22**, 579 (1961); S. Weinberg, Phys. Rev. Lett. **19**, 1264 (1967); A. Salam, Proc. 8th NOBEL Symposium, ed. N. Svartholm (Almqvist and Wiksell, Stockholm, 1968), p. 367.
 - [2] S. Dawson *et al.*, *The Higgs Hunter's Guide*, 2nd ed., Frontiers in Physics Vol. **80** (Addison-Wesley, Reading MA, 1990).
 - [3] M. Carena *et al.*, Report of the Tevatron Higgs working group; FERMILAB-CONF-00-279-T; hep-ph/0010338; C. Balazs *et al.*, Phys. Rev. **D59**, 055016 (1999).
 - [4] J.L. Díaz-Cruz *et al.*, Phys. Rev. Lett. **80**, 4641 (1998).
 - [5] J. Lorenzo Diaz Cruz, AIP Conf. Proc. **1026**, 30 (2008).
 - [6] A. Djouadi, Phys. Rept. **459**, 1 (2008).
 - [7] V. D. Barger, J. L. Hewett and R. J. N. Phillips, Phys. Rev. D **41**, 3421 (1990).
 - [8] See for instance: B. Dobrescu, Phys. Rev. **D63**, 015004 (2001). See also, recent work on Little Higgs models: N. Arkani-Hamed, A. G. Cohen, E. Katz and A. E. Nelson, JHEP **0207**, 034 (2002). And for AdS/CFT Higgs models: R. Contino, Y. Nomura and A. Pomarol, Nucl. Phys. B **671**, 148 (2003); A. Aranda, J. L. Diaz-Cruz, J. Hernandez-Sanchez and R. Noriega-Papaqui, Phys. Lett. B **658**, 57 (2007)
 - [9] J. Brau *et al.* [ILC Collaboration], arXiv:0712.1950 [physics.acc-ph]; A. Djouadi, J. Lykken, K. Monig, Y. Okada, M.J. Oreglia and S. Yamashita, arXiv:0709.1893 [hep-ph]; T. Behnke *et al.* [ILC Collaboration], arXiv:0712.2356 [physics.ins-det].
 - [10] G. Guignard (editor) [The CLIC Study Team], preprint CERN-2000-008 (2000).
 - [11] S. Kanemura, S. Moretti, Y. Mukai, R. Santos and K. Yagyu, arXiv:0901.0204 [hep-ph].
 - [12] K. S. Babu and C. F. Kolda, Phys. Lett. B **451**, 77 (1999).
 - [13] J. L. Diaz-Cruz, R. Noriega-Papaqui and A. Rosado, Phys. Rev. D **71**, 015014 (2005).
 - [14] H. Fritzsch and Z. Z. Xing, Phys. Lett. B **555** (2003) 63.
 - [15] T. P. Cheng and M. Sher, Phys. Rev. D **35**, 3484 (1987).
 - [16] J. L. Diaz-Cruz, R. Noriega-Papaqui and A. Rosado, Phys. Rev. D **69**, 095002 (2004).
 - [17] J. L. Díaz-Cruz and M.A. Pérez, Phys. Rev. D **33**, 273 (1986); J. Gunion, G. Kane and J. Wudka, Nucl. Phys. B **299**, 231 (1988); A. Mendez and A. Pomarol, Nucl. Phys. B **349**, 369 (1991); E. Barradas *et*

- et al.*, Phys. Rev. D **53**, 1678 (1996); M. Capdequi Peyranere, H. E. Haber and P. Irulegui, Phys. Rev. D **44**, 191 (1991); S. Moretti and W. J. Stirling, Phys. Lett. B **347**, 291 (1995) [Erratum-ibid. B **366**, 451 (1996)]; A. Djouadi, J. Kalinowski and P. M. Zerwas, Z. Phys. C **70**, 435 (1996); S. Kanemura, Phys. Rev. D **61**, 095001 (2000); J. Hernández-Sánchez *et al.*, Phys. Rev. D **69**, 095008 (2004); E. Asakawa, S. Kanemura and J. Kanzaki, Phys. Rev. D **75**, 075022 (2007); A. Arhrib, R. Benbrik and M. Chabab, J. Phys. G **34**, 907 (2007); A. Arhrib, R. Benbrik and M. Chabab, Phys. Lett. B **644**, 248 (2007).
- [18] J. L. Díaz-Cruz, J. Hernández-Sánchez and J.J. Toscano, Phys. Lett. B **512**, 339 (2001).
- [19] J. L. Diaz-Cruz, J. Hernandez-Sanchez, S. Moretti and A. Rosado, Phys. Rev. D **77**, 035007 (2008) J. L. Diaz-Cruz, J. Hernandez-Sanchez, S. Moretti and A. Rosado, AIP Conf. Proc. **1026**, 138 (2008).
- [20] E. Barradas-Guevara, O. Félix-Beltrán, J. Hernández-Sánchez and A. Rosado, Phys. Rev. D **71**, 073004 (2005).
- [21] M. A. Pérez and A. Rosado, Phys. Rev. D **30**, 228 (1984); J. Gunion *et al.*, Nucl. Phys. B **294**, 621 (1987); J. L. Díaz-Cruz and O.A. Sampayo, Phys. Rev. D **50**, 6820 (1994); J. F. Gunion, Phys. Lett. B **322**, 125 (1994).
- [22] S. Moretti and K. Odagiri, Phys. Rev. D **55**, 5627 (1997); Phys. Rev. D **59**, 055008 (1999); F. Borzumati, J.-L. Kneur and N. Polonsky, Phys. Rev. D **60**, 115011 (1999); S. Moretti and D. P. Roy, Phys. Lett. B **470**, 209 (1999); D.J. Miller, S. Moretti, D.P. Roy and W.J. Stirling, Phys. Rev. D **61**, 055011 (2000); A. A. Barrientos Bendezu and B. A. Kniehl, Phys. Rev. D **59**, 015009 (1999); Phys. Rev. D **61**, 097701 (2000); Phys. Rev. D **63**, 015009 (2001); O. Brein and W. Hollik, Eur. Phys. J. C **13**, 175 (2000); O. Brein, W. Hollik and S. Kanemura, Phys. Rev. D **63**, 095001 (2001); M. Bisset, M. Guchait and S. Moretti, Eur. Phys. J. C **19**, 143 (2001); Z. Fei *et al.*, Phys. Rev. D **63**, 015002 (2001); A. Belyaev, D. Garcia, J. Guasch and J. Sola, JHEP **0206**, 059 (2002); Phys. Rev. D **65**, 031701 (2002); M. Bisset, F. Moortgat and S. Moretti, Eur. Phys. J. C **30**, 419 (2003); Q. H. Cao, S. Kanemura and C. P. Yuan, Phys. Rev. D **69**, 075008 (2004); E. Asakawa, O. Brein and S. Kanemura, Phys. Rev. D **72**, 055017 (2005); E. Asakawa and S. Kanemura, Phys. Lett. B **626**, 111 (2005).
- [23] A. Abulencia *et al.* [CDF Collaboration], Phys. Rev. Lett. **96**, 042003 (2006).
- [24] For a review see: F. Borzumati and A. Djouadi, Phys. Lett. B **549**, 170 (2002); D. P. Roy, Mod. Phys. Lett. A **19**, 1813 (2004).
- [25] C. Amsler *et al.* [Particle Data Group], Phys. Lett. B **667**, 1 (2008).
- [26] S. Kanemura, T. Kubota and E. Takasugi, Phys. Lett. B **313**, 155 (1993); J. Horejsi and M. Kladiva, Eur. Phys. J. C **46**, 81 (2006); A. G. Akeroyd, A. Arhrib and E. M. Naimi, Phys. Lett. B **490**, 119 (2000).
- [27] H. J. He and C. P. Yuan, Phys. Rev. Lett. **83**, 28 (1999).
- [28] Y. B. Dai, C. S. Huang, J. T. Li and W. J. Li, Phys. Rev. D **67**, 096007 (2003); Z. J. Xiao and L. P. Yao, Commun. Theor. Phys. **38**, 683 (2002). C. L. Lin, C. E. Lee and Y. W. Yang, Phys. Rev. D **50**, 558 (1994).
- [29] A. E. Carcamo, R. Martinez and J. A. Rodriguez, Eur. Phys. J. C **50**, 935 (2007). R. A. Diaz, R. Mar-

- tinez and J. Alexis Rodriguez, arXiv:hep-ph/0103307; Phys. Rev. D **64**, 033004 (2001); Phys. Rev. D **63**, 095007 (2001).
- [30] B. Dudley and C. Kolda, arXiv:0901.3337 [hep-ph].
 - [31] F. Borzumati and C. Greub, Phys. Rev. D **59**, 057501 (1999).
 - [32] Z. J. Xiao and L. Guo, Phys. Rev. D **69**, 014002 (2004).
 - [33] N. G. Deshpande, P. Lo, J. Trampetic, G. Eilam and P. Singer, Phys. Rev. Lett. **59**, 183 (1987).
 - [34] D. Bowser-Chao, K. m. Cheung and W. Y. Keung, Phys. Rev. D **59**, 115006 (1999) [arXiv:hep-ph/9811235].
 - [35] A. Wahab El Kaffas, P. Osland and O. M. Ogreid, Phys. Rev. D **76**, 095001 (2007) [arXiv:0706.2997 [hep-ph]].
 - [36] G. Isidori, arXiv:0710.5377 [hep-ph].
 - [37] J. L. Diaz-Cruz *et al.*, in preparation.
 - [38] P. H. Chankowski, M. Krawczyk and J. Zochowski, Eur. Phys. J. C **11**, 661 (1999) [arXiv:hep-ph/9905436].
 - [39] J. L. Diaz-Cruz, H. J. He and C. P. Yuan, Phys. Lett. B **530**, 179 (2002).
 - [40] S. Dittmaier, G. Hiller, T. Plehn and M. Spannowsky, Phys. Rev. D **77**, 115001 (2008).
 - [41] J. Pumplin *et al.*, JHEP **207**, 12 (2002); D. Stump *et al.*, arXiv:hep-ph/0303013.
 - [42] M. Guchait and S. Moretti, JHEP **0201**, 001 (2002).
 - [43] F. Borzumati, J.-L. Kneur and N. Polonsky, in Ref. [22].
 - [44] D.J. Miller, S. Moretti, D.P. Roy and W.J. Stirling, in Ref. [22].
 - [45] S. Moretti and D. P. Roy, in Ref. [22].
 - [46] D. Cavalli *et al.*, hep-ph/0203056.
 - [47] K. A. Assamagan *et al.*, in Ref. [17].
 - [48] J. Alwall, C. Biscarat, S. Moretti, J. Rathsmann and A. Sopczak, Eur. Phys. J. C **39S1**, 37 (2005).
 - [49] S. Moretti, Pramana **60**, 369 (2003).
 - [50] K. A. Assamagan, M. Guchait and S. Moretti, hep-ph/0402057.
 - [51] G. Abbiendi, I. G. Knowles, G. Marchesini, M. H. Seymour, L. Stanco and B. R. Webber, Comp. Phys. Commun. **67**, 465 (1992).
 - [52] G. Corcella *et al.*, JHEP **0101**, 010 (2001).
 - [53] G. Corcella *et al.*, hep-ph/9912396, hep-ph/0107071, hep-ph/0201201 and hep-ph/0210213.
 - [54] S. Moretti, K. Odagiri, P. Richardson, M. H. Seymour and B. R. Webber, JHEP **0204**, 028 (2002).
 - [55] T. Sjöstrand, Comp. Phys. Comm. **82**, 74 (1994); T. Sjöstrand, P. Edén, C. Friberg, L. Lönnblad, G. Miu, S. Mrenna and E. Norrbin, Comp. Phys. Commun. **135**, 238 (2001); T. Sjöstrand, L. Lönnblad and S. Mrenna, hep-ph/0108264; T. Sjöstrand, L. Lönnblad, S. Mrenna and P. Skands, hep-ph/0308153.
 - [56] J. Alwall and J. Rathsmann, JHEP **0412**, 050 (2004).
 - [57] S. Moretti, J. Phys. G **28**, 2567 (2002).